European Journal of Immunology

Immunodeficiencies and autoimmunity

Clinical

Research Article

Follicular helper T cell signature of replicative exhaustion, apoptosis, and senescence in common variable immunodeficiency

Giulia Milardi[1], *Biagio Di Lorenzo*[1], *Jolanda Gerosa*[1], *Federica Barzaghi*[2,3], *Gigliola Di Matteo*[4,5], *Maryam Omrani*[3,6], *Tatiana Jofra*[1], *Ivan Merelli*[3,7], *Matteo Barcella*[3], *Matteo Filippini*[1], *Anastasia Conti*[3], *Francesca Ferrua*[2,3], *Francesco Pozzo Giuffrida*[2,3], *Francesca Dionisio*[3], *Patrizia Rovere-Querini*[8], *Sarah Marktel*[9], *Andrea Assanelli*[9], *Simona Piemontese*[9], *Immacolata Brigida*[3], *Matteo Zoccolillo*[3], *Emilia Cirillo*[10], *Giuliana Giardino*[10], *Maria Giovanna Danieli*[11], *Fernando Specchia*[12], *Lucia Pacillo*[4,5], *Silvia Di Cesare*[4,5], *Carmela Giancotta*[4,5], *Francesca Romano*[13], *Alessandro Matarese*[14], *Alfredo Antonio Chetta*[15], *Matteo Trimarchi*[16,23], *Andrea Laurenzi*[1], *Maurizio De Pellegrin*[17], *Silvia Darin*[2], *Davide Montin*[18], *Maddalena Marinoni*[19], *Rosa Maria Dellepiane*[20], *Valeria Sordi*[1], *Vassilios Lougaris*[21], *Angelo Vacca*[22], *Raffaella Melzi*[1], *Rita Nano*[1], *Chiara Azzari*[13], *Lucia Bongiovanni*[23], *Claudio Pignata*[10], *Caterina Cancrini*[4,5], *Alessandro Plebani*[21], *Lorenzo Piemonti*[1,24], *Constantinos Petrovas*[25], *Raffaella Di Micco*[3], *Maurilio Ponzoni*[23,24], *Alessandro Aiuti*[2,3,24], *Maria Pia Cicalese*[2,3] and *Georgia Fousteri*[1]

[1] Division of Immunology, Transplantation, and Infectious Diseases, Diabetes Research InstituteIRCCS San Raffaele Hospital, Via Olgettina 60, Milan, 20132, Italy
[2] Pediatric Immunohematology and Bone Marrow Transplantation Unit, IRCCS San Raffaele Hospital, Via Olgettina 60, Milan, 20132, Italy
[3] Pathogenesis and therapy of primary immunodeficiencies Unit, San Raffaele Telethon Institute for Gene TherapySr-TIGETIRCCS San Raffaele Hospital, Via Olgettina 60, Milan, 20132, Italy
[4] Department of Systems Medicine, University of Rome Tor Vergata, Via Cracovia 50, Rome, 00133, Italy
[5] Immune and Infectious Diseases Division, Research Unit of Primary Immunodeficiencies, Academic Department of Pediatrics, Bambino Gesù Children's HospitalIRCCS, Piazza di Sant'Onofrio 4, Rome, 00165, Italy
[6] Department of Computer Science, Systems and Communication, University of Milano-Bicocca, Piazza dell'Ateneo Nuovo 1, Milan, 20126, Italy
[7] Department of Bioinformatics, Institute for Biomedical TechnologiesNational Research Council, Via Fratelli Cervi 93, Segrate, 20090, Italy
[8] Department of Immunology, Transplantation and Infectious DiseasesIRCCS San Raffaele Hospital, Via Olgettina 60, Milan, 20132, Italy
[9] Hematology and Bone Marrow Transplantation Unit, IRCCS San Raffaele Hospital, Via Olgettina 60, Milan, 20132, Italy
[10] Department of Translational Medical Sciences, Section of PediatricsFederico II University of Naples, Corso Umberto I, 40, 80138, Italy
[11] Department of Clinical and Molecular Sciences, Marche Polytechnic University of AnconaClinica Medica, Via Tronto 10/a, Ancona, 60126, Italy
[12] Department of Pediatrics, S. Orsola-Malpighi HospitalUniversity of Bologna, Via Giuseppe Massarenti 9, Bologna, 40138, Italy

Correspondence: Georgia Fousteri
e-mail: fousteri.georgia@hsr.it

[Correction added on 25 November 2022, after first online publication: BIBLIOSAN funding statement has been added.]

[13] Pediatric Immunology Division, Department of Pediatrics, Anna Meyer Children's University Hospital, Viale Gaetano Pieraccini 24, Florence, 50139, Italy
[14] Department of Respiratory Medicine, Santi AntonioBiagio and Cesare Arrigo Hospital, Via Venezia 16, Alessandria, 15121, Italy
[15] Department of Medicine and Surgery, Respiratory Disease and Lung Function UnitUniversity of Parma, Str. dell'Università 12, Parma, 43121, Italy
[16] Otorhinolaryngology Unit, Head and Neck Department, IRCCS San Raffaele Scientific Institute, Via Olgettina 60, Milan, 20132, Italy
[17] Unit of Orthopaedics, IRCCS San Raffaele Scientific Institute, Via Olgettina 60, Milan, 20132, Italy
[18] Department of Pediatrics and Public Health, Regina Margherita Hospital, Piazza Polonia 94, Turin, 10126, Italy
[19] Pediatric Unit, Ospedale "F. Del Ponte", Via Filippo del Ponte 19, Varese, 21100, Italy
[20] Department of Pediatrics, Fondazione IRCCS Cà Granda Ospedale Maggiore PoliclinicoUniversity of Milan, Via Francesco Sforza 35, Milan, 20122, Italy
[21] Department of Clinical and Experimental Sciences, Pediatrics Clinic and Institute for Molecular Medicine A. NocivelliUniversity of Brescia, Piazza del Mercato 15, Brescia, 25121, Italy
[22] Department of Biomedical Sciences and Human Oncology, University of Bari Medical School, Piazza Umberto I, 1, Bari, 70121, Italy
[23] Pathology Unit, IRCCS San Raffaele Hospital, Via Olgettina 60, Milan, 20132, Italy
[24] Faculty of Medicine, University Vita-Salute San Raffaele, Via Olgettina 60, Milan, 20132, Italy
[25] Tissue Analysis Core, Immunology Laboratory, Vaccine Research CenterNational Institute of Allergy and Infectious DiseasesNational Institutes of Health, 9000 Rockville Pike, Bethesda, MD, 20892, USA

Common variable immunodeficiency (CVID) is the most frequent primary antibody deficiency whereby follicular helper T (Tfh) cells fail to establish productive responses with B cells in germinal centers. Here, we analyzed the frequency, phenotype, transcriptome, and function of circulating Tfh (cTfh) cells in CVID patients displaying autoimmunity as an additional phenotype. A group of patients showed a high frequency of cTfh1 cells and a prominent expression of PD-1 and ICOS as well as a cTfh mRNA signature consistent with highly activated, but exhausted, senescent, and apoptotic cells. Plasmatic CXCL13 levels were elevated in this group and positively correlated with cTfh1 cell frequency and PD-1 levels. Monoallelic variants in *RTEL1*, a telomere length- and DNA repair-related gene, were identified in four patients belonging to this group. Their blood lymphocytes showed shortened telomeres, while their cTfh were more prone to apoptosis. These data point toward a novel pathogenetic mechanism in CVID, whereby alterations in DNA repair and telomere elongation might predispose to antibody deficiency. A Th1, highly activated but exhausted and apoptotic cTfh phenotype was associated with this form of CVID.

Keywords: B cells · Common variable immunodeficiency · Immune aging · T-cell exhaustion · T follicular helper cells

Additional supporting information may be found online in the Supporting Information section at the end of the article.

Introduction

Common variable immunodeficiency (CVID) is the most common primary antibody deficiency (PAD) in humans. CVID is characterized by low levels of IgG, IgA, and/or IgM, failure to produce antigen-specific antibodies, and accounts for the majority (57%) of symptomatic primary immunodeficiencies according to the European Society for Immunodeficiencies registry [1–3], with estimated prevalence at 1 in 20.000–50.000 new births (www.esid.org). Secondary clinical features of CVID include combinations of various infectious, autoimmune and lymphoproliferative manifestations that complicate the course and the management of the disease. Mortality increases by 11-fold if any secondary clinical feature is present, with an overall survival considerably lower than the general population [4]. Ig supply is the mainstay of treatment for CVID that is often combined with immunomodulatory drugs to improve the management of secondary complications [5]. Different autoimmune (AI)

manifestations often coincide in the same CVID patient and their management remains a great challenge [6].

Failure of antibody production in CVID can be the direct result of B-cell insufficiency and dysfunction or can be T-cell mediated. For instance, a reduction in the number and percentage of isotype-switched B cells [7, 8], as well as a loss of plasma cells in the bone marrow and mucosal tissues, has been reported [9]; on the other hand, T follicular helper (Tfh) cells, which drive T-cell-dependent humoral immunity in germinal centers (GCs), were shown to underpin CVID development in some patients [10]. A predominant Th1 phenotype and altered Tfh function have been described in patients affected by CVID with various manifestations of immune dysregulation [11]. Follicular regulatory T cells (Tfr) safeguard the function of Tfh cells limiting AI and excessive GC reactions. The role of Tfr cells in CVID remains unexplored: these cells could be dysfunctional promoting AI or hyperactive overinhibiting Tfh cells and ultimately leading to CVID.

Next-generation sequencing has led to the discovery of an increasing number of monogenic causes of CVID [12, 13]. In the small list of monogenic CVID disorders, mutations in Tfh-associated genes such as *ICOS* [14–16], *IL-21* [15, 16], SLAM family proteins [17], and others [18] reduce the number or function of Tfh cells. Moreover, activated circulating Tfh cells have been associated with the immune phenotype of patients affected by AI diseases and underpin the production of autoantibodies (AAb) [19–22]. On these grounds, we analyzed the frequency, subset distribution, phenotype, transcriptome, and function of Tfh cells in 27 patients with CVID presenting AI as a secondary phenotype. We also investigated Tfr cells and B cells for their frequency and phenotype and determined CXCL13 plasma levels. Finally, we performed whole-exome sequencing (WES) in a fraction of patients and identified mutations and genetic variants that could account for the development of CVID and their Tfh-related immunophenotype.

Results

CVID patients show prevalence of Th1 circulating follicular helper T cells

We studied the frequency and subset distribution of circulating Tfh (cTfh) and Tfr (cTfr) cells in the peripheral blood of a cohort of 27 patients (16 adults and 11 pediatrics) with CVID (Table 1, Fig. 1). None of the patients had a genetic diagnosis at the time of recruitment. Patients were compared to 106 age- and sex-matched healthy controls (HC) (Table 1). cTfh ($CXCR5^+FoxP3^-$), cTfr ($CXCR5^+FoxP3^+$), and cTreg ($CXCR5^-FoxP3^+$) cell frequencies were determined on isolated peripheral blood mononuclear cells (PBMC) (Fig. 2A and Supporting Information Fig. S1A, gating strategy in this article's Online Repository). cTfh cells expressed low or intermediate CD45RA levels suggesting they were antigen-experienced (Supporting Information Fig. S1B). The frequency of cTfh cells observed in patients was higher than in HC but quite heterogeneous (median 13.90% in CVID vs. 10.90% in HC; $p = 0.0132$) (Fig. 2B). Three patients had a cTfh cell frequency below the lowest value seen in HC (3.84%), while four patients had a cTfh cell frequency above the higher value observed in HC (23.30%) (Fig. 2B). The remaining patients had a cTfh cell frequency similar to HC (Fig. 2B). No significant difference was observed in the frequency of cTfr cells (median 1.48% in CVID vs. 1.47% in HC; $p = 0.5407$) (Fig. 2C). Accordingly, blood cTfh: cTfr cell ratio was higher in CVID patients in comparison to HC (median 9.56 in CVID vs. 7.41 in HC; $p = 0.0449$) (Fig. 2D). CXCR5-neg Tconv to CXCR5-neg Treg ratio was similar between patients and HC (data not shown).

Three human cTfh subsets can be defined according to the differential expression of CXCR3 and CCR6: $CXCR3^+CCR6^-$ cTfh1 cells, $CXCR3^-CCR6^-$ cTfh2 cells, and $CXCR3^-$ $CCR6^+$ cTfh17 cells (Supporting Information Fig. S1C) [23, 24]. Our cohort of CVID patients had a significantly higher percentage of cTfh1 cells as compared to HC (median 42.50% in CVID vs. 27.705 in HC; $p = 0.0002$) (Fig. 2E), in line with previous reports [12, 25, 26]. The percentage of cTfh17 cells was lower in CVID patients as compared to HC (median 13.40% in CVID vs. 25.70% in HC; $p < 0.0001$) (Fig. 2F), also the proportion of cTfh2 cells was significantly different between CVID and HC (median 28.10% in CVID vs. 37.20% in HC; $p = 0.0155$) (Fig. 2G).

We also assessed the frequency of peripheral blood B cell subsets defined by the expression of CD21, CD38, CD24, CD27, and Ig markers in 8 CVID patients and 90 age- and sex-matched HC (Supporting Information Fig. S2A,B for gating strategy). The frequency of circulating $CD19^+$ B cells (median 1.48% in CVID vs. 10.10% in HC; $p < 0.0001$) (Supporting Information Fig. S2C), memory B cells ($CD19^+CD27^+$) (median 7.89% in CVID vs. 17% in HC; $p = 0.0062$) (Supporting Information Fig. S2E), mature memory B cells (median 2.54% in CVID vs. 12.92% in HC; $p < 0.0001$) (Fig. E2,J), $CD27^+IgG^+$ B cells (median 7.24% in CVID vs. 12.50% in HC; $p = 0.0709$) (Supporting Information Fig. S2H) and, $CD27^+IgA^+$ cells (0% in CVID vs. 10.20% in HC; $p = 0.0056$) (Supporting Information Fig. S2I) was reduced in the tested patients as compared to HC. No significant differences were observed in the percentage of $CD19^+CD27^-$ naive B cells (median 89.40% in CVID vs. 82.10% in HC; $p = 0.0507$) (Supporting Information Fig. S2D), $CD38^{hi}CD24^{hi}$ transitional B cells (median 4.74% in CVID vs. 7.64% in HC; $p = 0.3265$) (Supporting Information Fig. S2F), and SM B cells (median 4.35% in CVID vs. 8.18% in HC; $p = 0.1129$) (Supporting Information Fig. S2G), as well. Additionally, CVID patients showed a lower percentage of $CD21^{lo}CD38^{lo}$ B cells (median 1.59% in CVID vs. 2.15% in HC; $p = 0.7700$) (Supporting Information Fig. S2K), and an elevated frequecy of plasma cells (median 10.20% in CVID vs. 0.53% in HC; $p < 0.0001$) (Supporting Information Fig. S2L).

Predominance of a $cTfh1^{hi}Tfh17^{lo}PD\text{-}1^{hi}CXCL13^{hi}$ immunophenotype in a group of CVID patients

PD-1 and ICOS are the main markers of Tfh cell activation and are considered indicators of their functional status [27]. Here,

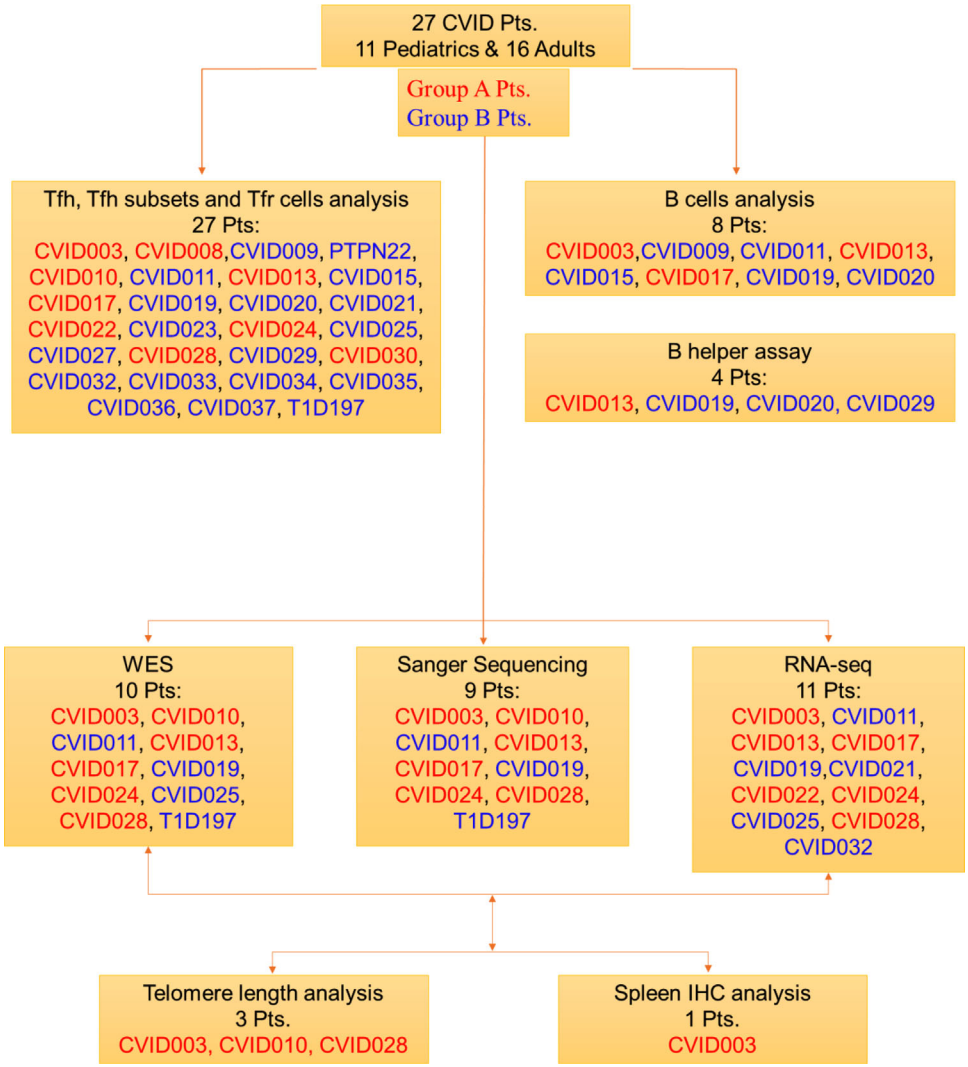

Figure 1. Flow chart showing the different studies performed in peripheral blood of a cohort of 27 patients (16 adults and 11 pediatrics) with CVID.

we analyzed PD-1- and ICOS-expression by cTfh cells, and the proportion of the highly functional (HF) cTfh subset ($CXCR3^{-}PD\text{-}1^{+}$). Overall, cTfh cells from CVID patients showed an increased expression of PD-1 (median 40.50 in CVID vs. 21.55 in HC, $p < 0.0001$) and ICOS (median 2.60 in CVID vs. 1.35 in HC, $p = 0.0009$) as compared to HC (Fig. 3A–C). A significant fraction of $PD\text{-}1^{+}$ cTfh cells was also $CXCR3^{-}$ and, consequently, the percentage of HF cTfh cells was higher in patients when compared to HC (median 11.80 in CVID vs. 10.15 in HC; $p = 0.0367$) (Fig. 3D). The elevated expression of PD-1 was not restricted to the $CXCR3^{-}$ cTfh population as $CXCR3^{+}$ cTfh, Tfr, and Treg cells also showed elevated PD-1 expression (data not included).

CVID patients were also characterized by an elevated plasma CXCL13 level as compared to HC (median 196.1 pg/mL in CVID vs. 47.68 pg/mL in HC; $p < 0.0001$) (Fig. 3E). Furthermore, a significant correlation between CXCL13 plasma levels and the percentage of cTfh1 (Fig. 3F) and cTfh17 (Fig. 3G) subsets was seen in patients. In addition, CXCL13 levels correlated positively with the PD-1 levels expressed by CVID cTfh cells (Fig. 3H).

Based on these findings, we thought to distinguish CVID patients into two groups. We used two criteria: the frequency of cTfh1 cells and used as cut-off a >40% value, the higher value observed in our HC cohort (Fig. 4A), and the plasma levels of CXCL13 (>300 pg/mL) (Fig. 4B). A total of $n = 9$ patients fulfilled both criteria (Group A). As expected, the frequency of cTfh17 was in the lower range for this group of patients, below the lower cut-off value seen in HC (Fig. 4C). The majority of cTfh cells of this group also expressed high levels of PD-1 (Fig. 4D). The rest of the patients were included in Group B ($n = 18$). Hence, based on the frequency of cTfh1 cells and plasma CXCL13 levels, we identified two groups of CVID patients, Group A with a prevalence of $cTfh1^{hi}Tfh17^{lo}PD\text{-}1^{hi}CXCL13^{hi}$ immunophenotype and Group B, with a Tfh-related immunophenotype that was more similar to HC (Fig. 4E).

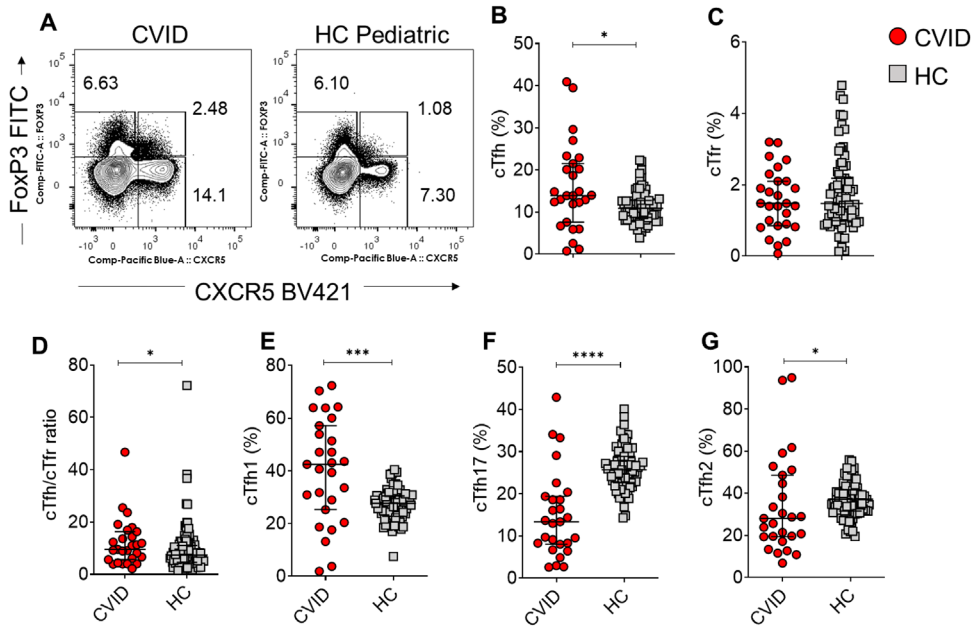

Figure 2. Flow cytometry analysis of circulating follicular helper T (cTfh) cells and their subsets in peripheral blood samples from common variable immunodeficiency and autoimmunity (CVID) patients with respect to controls (HC). (A) Representative flow cytometry plots for Tfh ($CXCR5^+CD4^+$), follicular Treg ($FoxP3^+CXCR5^-$), and conventional Treg ($CXCR5^-CD4^+$), gated on singlets lymphocytes, $CD3^+CD14^-CD8^-CD19^-$. Percentages of cTfh (B), cTfr (C), cTfh:cTfr ratio (D), and cTfh subsets in peripheral blood of CVID patients compared to age-matched HC. From left to right: (E) frequencies of cTfh1 subset ($CXCR3^+$ $CCR6^-$), (F) cTfh17 ($CXCR3^-$ $CCR6^+$), (G) cTfh2 ($CXCR3^-$ $CCR6^-$). Data are pooled from more than 10 independent experiments (CVID $n = 27$, HD $n = 106$). In all graphs, dots represent individual donors and asterisks indicate statistical significance as calculated by Mann–Whitney test. Black bars: median with interquartile range. $^*p < 0.05$; $^{**}p < 0.005$; $^{***}p < 0.001$; $^{****}p < 0.0001$.

To better analyze the functionality of CVID-derived cTfh cells and to see whether there were any differences between Group A and B, we performed co-cultures with either naive ($CD27^+$ $CD38^-$ $CD19^+$, B_N) or memory ($CD27^+$ $CD38^-$ $CD19^+$, B_M) FACS-sorted B cells. The in vitro functionality of cTfh cells was assessed in autologous settings, where both cTfh and B cells were derived from the same CVID patient, and in heterologous settings, where cTfh were co-cultured with B cells from HC. B cell differentiation into plasmablast, and IgM and IgG production were evaluated on Day 7 of culture. Group A CVID Tfh cells showed reduced ability to induce autologous B differentiation into plasmablast compared to Group B CVID and HC (Fig. 4F). IgG was almost undetectable in all CVID cTfh: B cell co-cultures irrespective the type of B cells (both group A and B) (Fig. 4G). Interestingly, B_N and B_M cells from CVID patients were able to secrete some IgM when co-cultured with autologous cTfh cells (Fig. 4H). Group A CVID cTfh cells were unable to induce plasmablast differentiation and IgG production when co-cultured with heterologous HC-derived B_N cells (Fig. 4I–K).

Next, we assessed the cytokine and chemokine plasma profile in some Group A ($n = 5$) and Group B ($n = 3$) CVID patients (Supporting Information Fig. S3). A stronger Tfh1 cell signature (IFN-γ, IP-10, IL-1β, and IL-18) was observed in the majority of Group A CVID patients when compared to Group B CVID patients (Supporting Information Fig. S3A). Group A patients were also characterized by significantly higher plasma concentrations of chemoattractant proteins CXCL13 and CXCL9 (Supporting Information Fig. S3B). BAFF, APRIL, CD30, CD40L (Supporting Information Fig. S3C), IL-2R (CD25), GCSF, and inflammatory proteins MDC and MIP3a (Supporting Information Fig. S3D) were also higher in the plasma of some CVID Group A patients. Other cytokines and chemokines were similar between the two groups (Supporting Information Fig. S3E).

Clinically, all patients in Group A displayed splenomegaly and lymphadenopathy as compared to Group B (Table 2). The prevalence of autoimmune cytopenia, granulomatous disease or enteropathy did not differ between the groups. Hence, we have identified a group of patients characterized by a predominant $cTfh1^{hi}Tfh17^{lo}PD\text{-}1^{hi}CXCL13^{hi}$ immunophenotype who, clinically, had a high prevalence of splenomegaly and lymphadenopathy.

Tfh transcriptional signature of hyperactivated yet exhausted and apoptotic cells in CVID

Next, we compared the overall transcriptomic landscape of FACS-purified $CD4^+CXCR5^+CD25^-$ cTfh cells from Group A ($cTfh1^{high}CXCL13^{high}$), Group B ($cTfh1^{normal}$ and $CXCL13^{normal}$) CVID patients and compared them to HC. Unbiased clustering analysis of the RNA seq data was followed by differential gene expression studies where Group A vs. B, Group A vs. HC, Group A vs. (B+HC), and Group B vs. HC were compared. Unbiased principal component analysis (PCA), distinguished CVID patients into two groups, Group A and B, that were the same ones

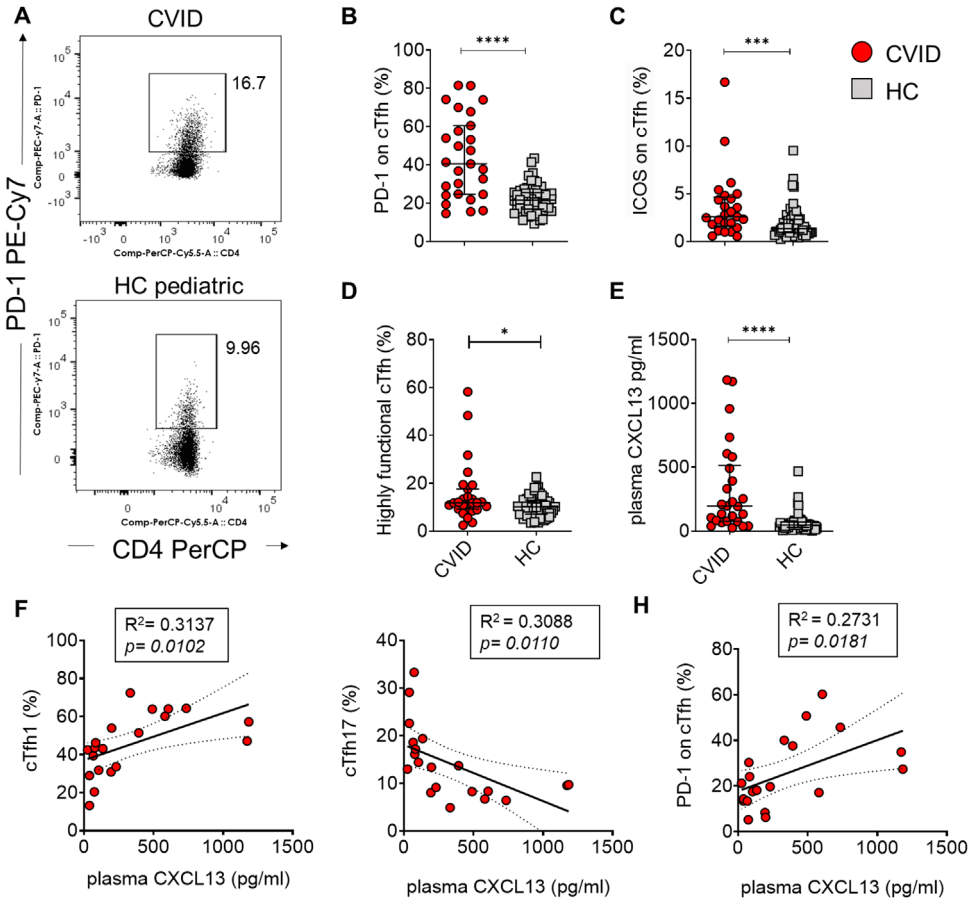

Figure 3. Programmed death (PD)-1 Inducible co-stimulator (ICOS) expression analysis on circulating Tfh cells in CVID patients compared to HC. Same donors as in Fig. 2 were analyzed. (A) Representative flow cytometry plots show PD-1 frequency on CVID patients and pediatric HC. (B,C) Percentages of PD-1 and ICOS on total cTfh. (D) Frequencies of Highly Functional cTfh ($CXCR3^-$ $PD\text{-}1^+$ $CXCR5^+$ $CD4^+$) cells. (E) CXCL13 levels (pg/mL) measured by ELISA assay in plasma of CVID patients compared to HC. Dots represent individual donors and asterisks indicate statistical significance as calculated by Mann–Whitney test. Black bars: median with interquartile range. $^*p < 0.05$; $^{**}p < 0.005$; $^{***}p < 0.001$; $^{****}p < 0.0001$. (F–H) Correlation analysis between CXCL13 plasma levels and frequencies of cTfh1, cTfh17, PD-1^+ on cTfh in CVID patients. Frequencies were analyzed by flow cytometry. Lines represent linear regression and SD. $^*p < 0.05$; $^{**}p < 0.005$; $^{***}p < 0.001$; $^{****}p < 0.0001$.

identified by phenotypical analysis (Supporting Information Fig. S4). 427 differentially expressed genes (DEGs) were identified by comparing cTfh cells of CVID Group A with HC, while comparison to CVID Group B identified solely 58 DEGs, of which 52 DEGS were present in the Group A vs. HC comparison. Hence, CVID Group A had a different Tfh expression profile compared to HC and the other CVID (Fig. 5A and Supporting Information Fig. S4B,C). Hierarchical group analysis for Tfh-related genes showed an increased expression of Tfh-highly active signature (e.g., IL-21, Bcl-6) in Group A CVID (Fig. 6B). Importantly, increased levels of CXCR5, CXCL13, and genes involved in Tfh lineage specification (as Bcl-6, IL-21, Tox2, ICOS, PD-1) had a strong influence on separating the two groups (Fig. 5B). Furthermore, additional hierarchical analysis that took into consideration T cell activation, exhaustion, and cell death pathways revealed an increased representation of these pathways in Group A CVID cTfh cells (Fig. 5C–E).

To address the exhaustion state of Group A CVID Tfh cells, we analyzed their cytokine expression profile. PBMC were activated with TPA and Ionomycin and the expression of IFN-γ, IL-17, IL-21, IL-10, IL-4 cytokines was evaluated by flow cytometry after gating on $CD4^+CXCR5^+$ cTfh cells. Except for one patient (CVID003), CVID Group A Tfh showed reduced expression of IFN-γ, IL-17, IL-21, IL-10 cytokines with respect to HC (Supporting Information Fig. S5) suggesting they were functionally exhausted.

Next, we investigated whether Tfh cells in Group A patients were more prone to apoptosis. $CD4^+CD45RA^-CXCR5^+$ Tfh, $CD4^+CD45RA^-CXCR5^-$ Tconv and $CD4^+CD45RA^+$ naïve T cells were FACS sorted from the peripheral blood and activated in vitro with anti-CD3/CD28 coated beads. Interestingly, Annexin-V/P.I. staining showed elevated cell death by Group A CVID cTfh and Tconv as compared to HC (calculated as fold-change). Impressively, naïve CD4 T cells showed a 250% increase on average in apoptosis as compared to HC naïve CD4 T cells (Fig. 6A,B).

Additional experiments on the same FACS-sorted cells (Tfh, Tconv, and naïve T cells) were carried out to determine their senescent profile. To identify senescent cells in culture, we

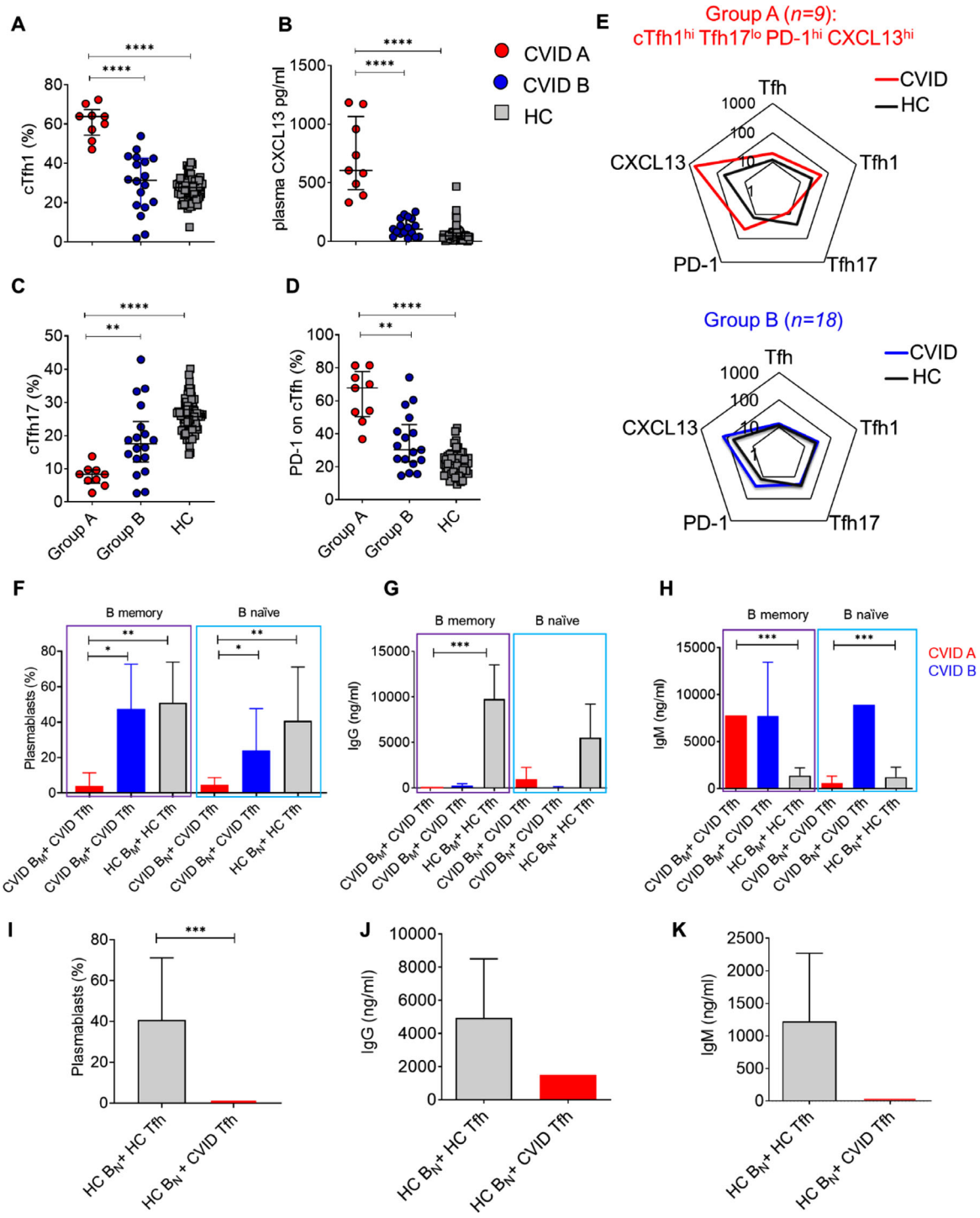

Figure 4. Two major categories of CVID patients based on Tfh-related markers. (A–D) Percentages of cTfh1, CXCL13, cTfh17, and PD-1 divide CVID patients in two groups: Group A cTfh1^{hi}Tfh17^{lo}PD-1^{hi}CXCL13^{hi} vs. Group B cTfh1/Tfh17/PD-1/CXCL13^{normal}. (E) Radar charts represent the percentage of cTfh, cTfh1, cTfh17, PD-1, and CXCL13 in CVID Group A vs. CVID Group B. (F) Frequency of plasmablasts (CD38^{hi} CD20^{-} CD19^{+}) after 1-week co-culture of autologous B memory (B_M) and B naïve (B_N) cells with autologous cTfh cells in CVID patients (donors per group A $n = 6$, and group B $n = 6$) compared to HC ($n = 6$). Data are pooled for five independent experiments. (G,H) IgG and IgM measured in ng/mL by ELISA assay in the supernatant of co-cultures after 1 week. (I) Percentages of plasmablasts (CD38^{hi} CD20^{-} CD19^{+}) after 1 week co-culture of autologous Tfh with heterologous B_N cells in CVID patients of Group A ($n = 4$) and Group B ($n = 6$) compared to HC ($n = 14$). (J,K) IgG and IgM production analyzed in ng/mL by ELISA assay in the supernatant of co-culture between autologous Tfh with heterologous B_N cells in Group A patient ($n = 1$) compared to HC ($n = 16$). Data are pooled from more than 10 independent experiments. Percentages were analyzed by flow cytometry. In all graphs, red dots and red bars represent individual donors of Group A, and blue dots and blue bars individual donors of Group B. Asterisks indicate statistical significance as calculated by Mann–Whitney test. Comparisons among > 2 groups were performed using the ANOVA test. Black bars: median with interquartile range. $^{*}p < 0.05$; $^{**}p < 0.005$; $^{***}p < 0.001$; $^{****}p < 0.0001$.

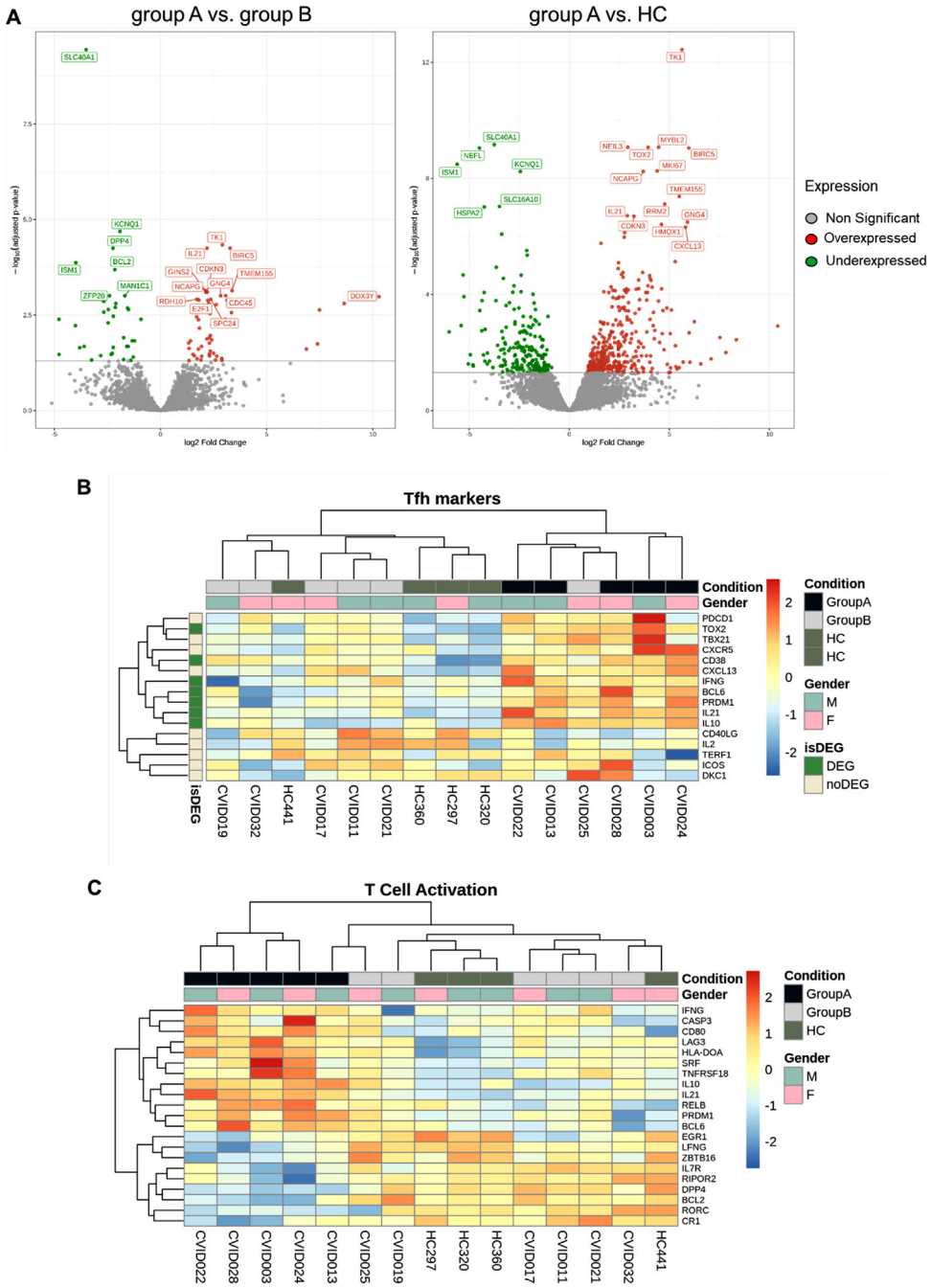

Figure 5. Transcriptomic landscape of sorted CD4$^+$CXCR5$^+$CD25$^-$ cTfh cells in CVID Group A ($n = 6$) vs. Group B ($n = 5$) patients vs. HC ($n = 4$) and their apoptotic profile. (A) Vulcano plots representing the gene expression profile of Group A ($n = 6$) vs Group B ($n = 5$) and Group A vs HC ($n = 4$). (B) Hierarchical grouping analysis based on Tfh-related genes divides patients into Tfh-highly active (Group A, $n = 6$) and normal (Group B, $n = 5$). Hierarchical grouping analysis representing the expression of genes involved in (C) T cell activation, (D) T cell exhaustion, and (E) cell death pathways. In the volcano plots and heat maps, red color intensities represent a higher gene expression. Data are pooled from more than three independent experiments.

induced the lysosomal alkalinization and stained them with the membrane-permeable compound C12FDG [28] and the cell cycle inhibitor p16 [29]. All populations increased the senescent markers SA-B galactosidase and p16, and we observed a marginal increase of senescence in CVID Group A cTfh and cTconv cells compared to HC (Fig. 6C–D).

Heterozygous variants in *RTEL1* are identified in group A CVID patients

WES analysis of genomic DNA in nine CVID patients (6 from Group A and 3 from Group B) identified 24 variants. Patients were prioritized on the basis of the severity of their clinical profile

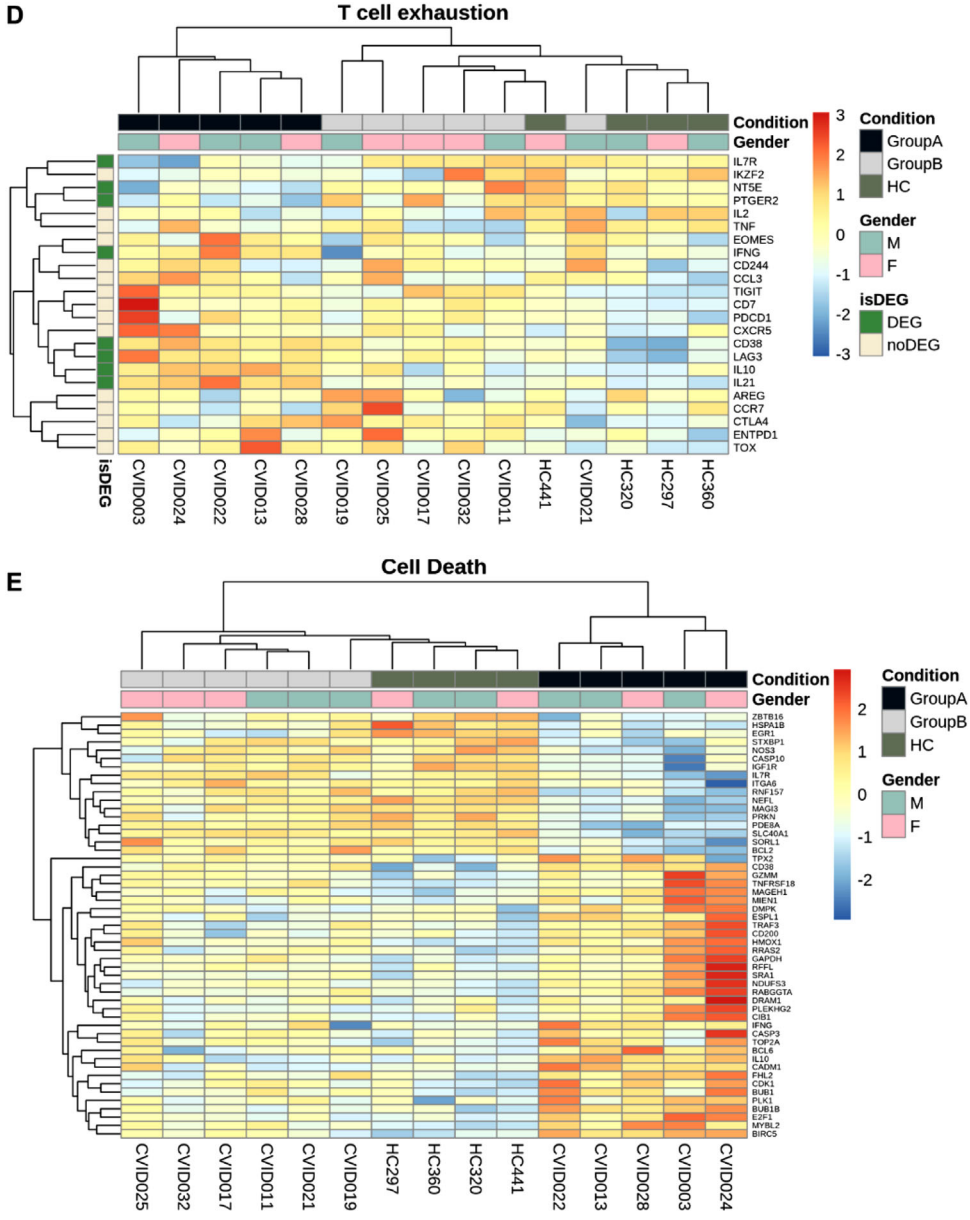

Figure 5. *Continued*

and immunophenotype. Variants were filtered for association with different forms of primary immunodeficiency including CVID (Supporting Information Table S1) [30]. A total of 16 variants were confirmed by Sanger sequencing in six patients (Table 3). Of these, heterozygous missense mutations in *RTEL1* gene (c.2785G>A, p.Ala929Thr; c.2123G>A, p.Arg708Gln; c.2051G>A, p. Arg684Gln; c.371A>G, p. Asn124Ser), which is essential for DNA replication, genome stability, DNA repair, and telomere maintenance [31–33] were observed in four out of five tested CVID patients belonging to Group A (Table 3). Group A patients with *RTEL1* variants had heterozygous variants in additional genes, i.e., in *PRF1* (c.273G>A, p.Ala91Val), *PRKDC* (c.9503C>T, p.Gly3149Asp), *STXBP2* (c.1331C>T, p.Ala444Val), *MST1* (c.1012T>C, p.Cys338Arg), *TNFRSF13B* (c.659T>C, p.Val220Ala), and *LYST* (c.2433C>T, p.Ser753Asn), suggesting that their disease was influenced by other variants in association to *RTEL1*. The immunological and clinical features of each patient are included in Supporting Information Table S2.

RTEL1 deficiency has recently been described as the major autosomic recessive etiology of dyskeratosis congenita (DKC), a rare disease that results from excessive telomere shortening and includes bone marrow failure, mucosal fragility, pulmonary or liver fibrosis, early-onset inflammatory bowel diseases, neurological impairment and, in more severe cases, immune deficiency and increased susceptibility to malignancies [32–35]. Accordingly, we evaluated telomere length in lymphocyte subsets isolated from

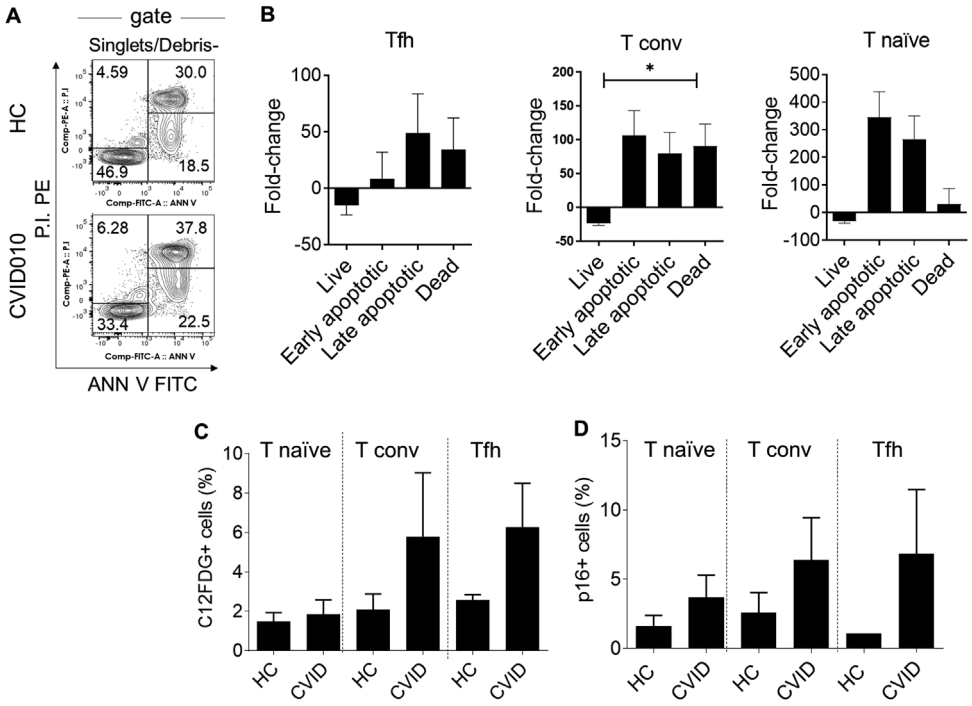

Figure 6. Flow cytometry analysis of apoptotic and senescent cells. (A) Representative gating strategy for live (ANN V$^-$ PI$^-$), early apoptotic (ANN V$^+$ PI$^-$), late apoptotic (ANN V$^+$ PI$^+$), and dead cells (ANN V$^-$ PI$^+$) after singlet selection and debris exclusion. (B) Flow cytometric analysis of live, early and late apoptotic, and dead cTfh, cTconv, and naïve cT cells. Data are shown as fold change from HC of the same experiment [(% CVID − % HC) / % HC]. Two independent experiments were performed with 1–2 HC and CVID donors each. (C–D) C12FDG (C) and p16 (D) indicate the percentage of senescent cells in CVID patients compared to HC. C12FDG and p16 stainings were performed on sorted T naïve, Tconv, and Tfh cells from peripheral blood. Asterisks indicate statistical significance as calculated by Mann–Whitney test. Comparisons among > 2 groups were performed using the ANOVA test. Black bars: median with interquartile range. $^*p < 0.05$; $^{**}p < 0.005$; $^{***}p < 0.001$; $^{****}p < 0.0001$.

three Group A patients, CVID003, CVID010, and CVID028 bearing, respectively, p.Ala929Thr, p.Arg708Gln, and p.Asn124Ser *RTEL1* heterozygous missense variants. Patient-derived lymphocytes had significantly shorter telomeres as compared to average control (Fig. 7A). CD45RA$^+$ naïve T cells, CD45RA$^-$ memory T cells, CD20$^+$ B cells, and CD57$^+$ NK cells exhibited shorter telomeres compared to control (Supporting Information Fig. S6).

Next, we sought to re-analyze the RNA-Seq data and perform a biased hierarchical grouping analysis focused on DNA damage and telomere length pathways. Higher expression of genes involved in DNA damage, telomere maintenance, and response to DNA damage were observed in cTfh cells from Group A as compared to Group B CVID patients (Fig. 7B,C). Comparison of RNAseq data for *RTEL1*, *TINF2*, *DKC1*, *TERT*, and *TERF1* expression levels, genes associated with DKC and Hoyeraal–Hreidarsson syndrome [36–41], showed no expression in Tfh cells (data not included). Next, we investigated *RTEL1* expression in GC Tfh cells, centroblasts (CB), and centrocytes (CC) sorted from tonsils. *RTEL1* was found expressed by tonsillar Tfh, CB and CC at mRNA levels that were comparable to HPRT (Fig. 7D and Supporting Information Fig. S7). Taken together, genetic analyses revealed the presence of heterozygous variants in *RTEL1* in four CVID Group A patients that clinically presented splenomegaly and lymphadenopathy while immunologically having high frequencies of cTfh1 expressing elevated levels of PD-1, and plasma CXCL13.

Splenic Tfh architecture in a patient with group A immunophenotype and a heterozygous variant in *RTEL1*

Patient CVID003 with a heterozygous variant in *RTEL1*, having short lymphocyte telomeres and a Group A Tfh cell immunophenotype developed splenomegaly (30 cm in maximum diameter) and underwent splenectomy. Macroscopic examination evidenced well-retained red pulp and pinpoint white pulp. Splenic parenchyma showed mild and plurifocal expansion of the white pulp with mild and focal congestion of the sinuses of the red pulp. In the subcapsular area, focal giant cell reaction of the foreign body type was associated with hemosiderin deposits (consistent with so-called 'Gandy-Gamma' nodules) (Supporting Information Fig. S8). In the white pulp, only focal reactive GCs (Bcl- 2 negative and high Ki-67 in centrofollicular cells) were seen containing an increased number of Tfh cells (CXCL13$^+$ PD-1$^+$), sometimes alternating with others with atrophic appearance (Fig. 8 and data not included). The marginal zone (IgD$^+$) was preserved (Supporting Information Fig. S8). In the interfollicular white pulp, CD4 T lymphocytes (CD3 $^+$, CD4 >> CD8) prevailed (data not included).

In line with the histological data, flow cytometry analysis of the splenic B cell subpopulation revealed a decrease in CD19$^+$ total B cells (7.5% in CVID003 vs. median 66.43% in HC), and a reduction in memory B cells (1.15% in CVID003 vs. median 5.62%

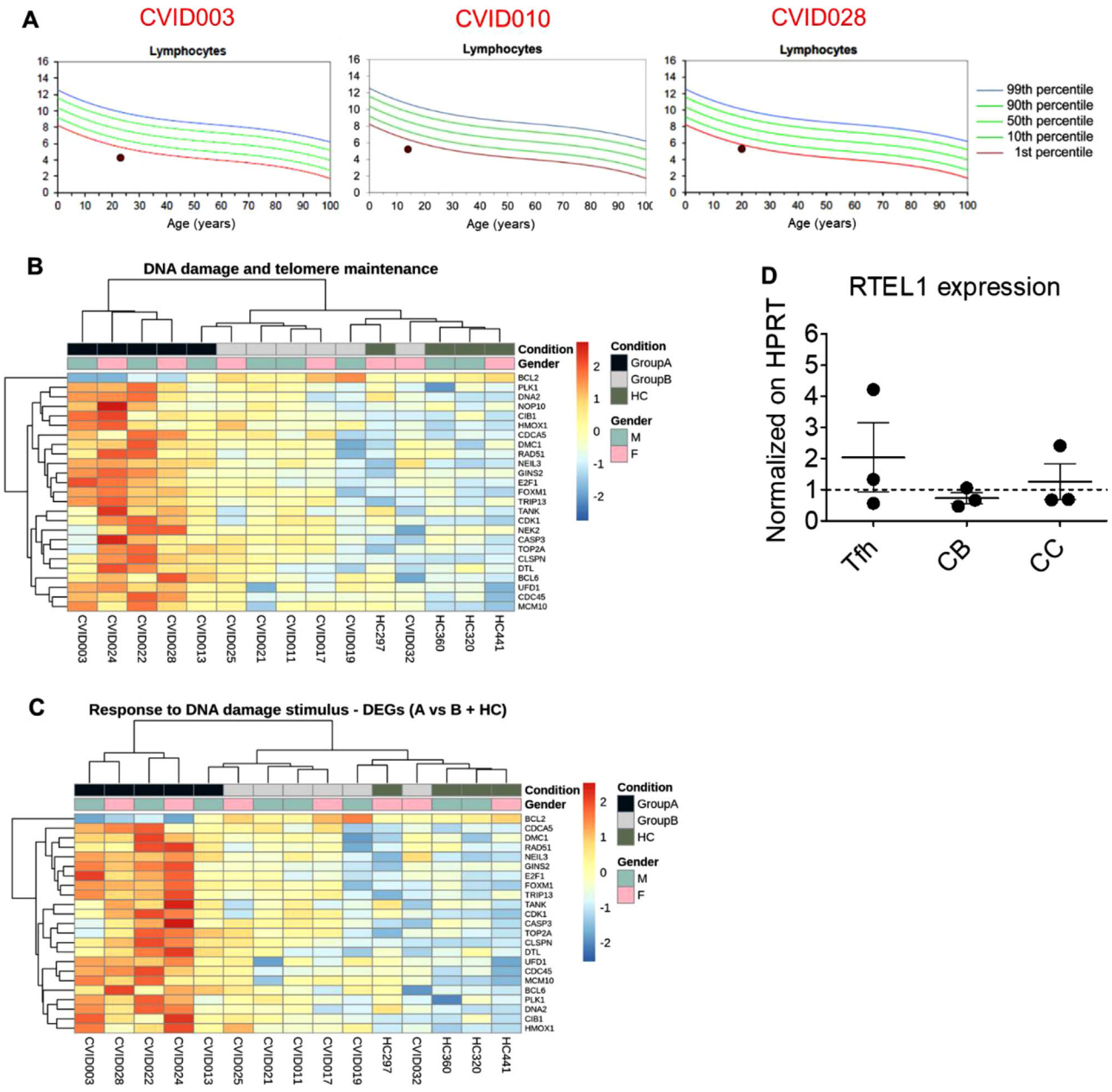

Figure 7. Telomere length and gene expression analysis in CVID patients. (A) Nomogram of Telomere Length (TL) in lymphocytes from three CVID patients of Group A, with percentile lines as annotated. Black dots represent CVID patients. Red, green, and blue slopes represent expected telomere length for the indicated proportion of HC. (B,C) Hierarchical grouping analysis of genes involved in telomere elongation and DNA damages pathways clusterize patients into Group A and Group B. Red color intensities represent a higher gene expression. (D) RTEL1 expression was assessed in sorted Tfh cells, CBs, and CCs from tonsillar samples ($n = 3$ donors). The average for technical duplicates was estimated, normalized on HPRT as a housekeeping gene, and represented as dark circles; HPRT expression (set at 1) is represented by the dotted line; mean and SD are also shown. Data are pooled from more than three independent experiments.

in HC) and plasma cells (0.62% in CVID003 vs. median 9.44% in HC) as compared to control spleens (Fig. 8B and Supporting Information Fig. S9, for additional B cell subset analysis). Percentage of age-related, CD21^{lo}CD38^{lo}, and transitional B cells were increased in the patient (35.7% in CVID003 vs. median 1.82% in HC) (Fig. 8B and Supporting Information Fig. S9). No IgA^{+} or IgG^{+} B cells could be detected (Fig. 8B). Furthermore, an increase in Ki67, a proliferation marker (13.5% in CVID003 vs. median 3.04% in HC) and Bcl-6 (4.72% in CVID003 vs. median 0.9% in HC) expression in B cells was observed (Fig. 8C).

Splenic CD4 and CXCR5^{+} Tfh cell frequencies were also higher in the patient as compared to control spleens (57.2% in CVID003 vs. median 9.78% in HC) (Fig. 8D and Supporting Information S10A), and expressed PD-1, Bcl-6, and CD57 at higher levels than

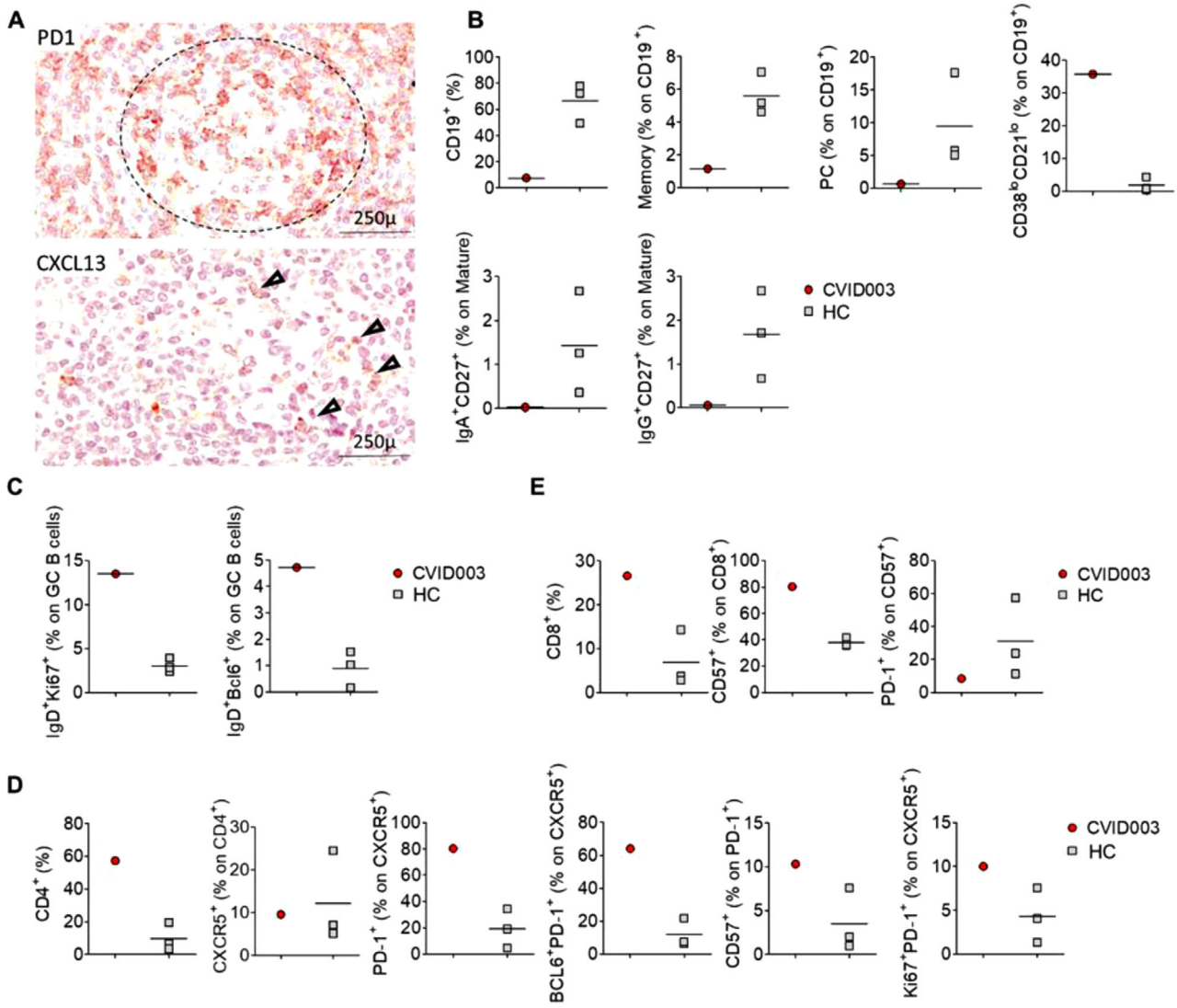

Figure 8. Germinal center detection in the patient's spleen. (A) Spleen histopathology of CVID003 patient with RTEL1 mutation. GCs revealed an increased number of Tfh as evidenced by CXCL13 (arrowhead) and PD-1 staining (dotted grey circle). Original magnification 400×. (B) Percentages of CD19+ B cells and their subsets: memory ($CD19^+CD27^+$) B cells, $CD21^{lo}$ B cells, plasma cells ($CD38^+CD24^-$), transitional B cells ($CD38^{hi}CD24^{hi}$), IgA^+CD27^+, IgG^+CD27^-, IgG^+CD27^+. (C) Frequencies of GC B cells expressing the proliferation markers as Ki67 and Bcl-6. (D) Percentages of $CD4^+CXCR5^+$ Tfh, and Tfh expressing PD-1, CD57 and Bcl-6 and Ki67 as proliferation marker in the spleen of CVID003 patient compared to age-matched HC. Percentages were analyzed by flow cytometry. Dots represent individual donors. Statistical significance was calculated by Mann–Whitney test.

the HC (PD-1: 80.20% in CVID003 vs. median 19.32% in HC; Bcl-6: 64.10% in CVID003 vs. median 11.96% in HC; CD57: 10.30% in CVID003 vs. median 3.51% in HC) (Fig. 8D and Supporting Information S10A). Ki-67 was also highly expressed by CVID003 Tfh cells (10% in CVID003 vs. median 4.31% in HC) (Fig. 8D and Supporting Information S10A). We also observed a higher frequency of CD8 T cells (26.60% in CVID003 vs. median 6.91% in HC) that also enriched in $CD57^+$ cells (80.30% in CVID003 vs. median 37.73% in HC). However, PD-1 expression levels were not increased in CD8 T cells in the spleen of the patient (8.34% in CVID003 vs. median 30.87% in HC) (Fig. 8E and Supporting Information S10B). These data corroborate with the majority of observations made in the blood suggesting that Tfh cells are present in Group A CVID but display a senescent and exhausted phenotype.

Discussion

This study unravels a group of CVID patients that markedly differ from the majority CVID patients and HC in their cTfh cell composition. Patients within this group showed a $cTfh1^{hi}Tfh17^{lo}PD\text{-}1^{hi}CXCL13^{hi}$ immunophenotype, a high Th1 plasma cytokine and chemokine polarization, and a cTfh-cell RNA signature consistent with highly activated but exhausted and apoptotic cells. Equally important, genetic analysis identified monoallelic variants and

polymorphisms in *RTEL1*, a helicase essential in DNA metabolism, in four patients belonging to this group, whose lymphocytes presented significantly shortened telomeres and were more senescent and prone to activation-induced cell death. These results were achieved by evaluating a broad array of GC-related immune markers in the blood of a subset of CVID patients presenting AI as a secondary complication exploiting a multifaceted investigative approach including flow cytometry, exome sequencing, and transcriptomic evaluation of cTfh cells. Hence, our findings indicate that heterozygous variants in DNA damage response and telomere elongation pathways could underlie CVID and be strongly linked to GC-associated immune dysregulation by a mechanism that involves premature immune aging. Taken together, our analyses provide support for a concept where a Tfh phenotype may be associated with a specific CVID endotype.

CVID is a collection of disorders of humoral dysregulation resulting in low IgG and sometimes IgM levels and antibody-specific responses with recurrent infections [39]. Previous studies have addressed the immunologic spectrum of CVID and identified B cell profiles that determine different forms of the disease [11]. Premature immune aging has been also described in a previous study where short telomeres and reduced T and B cell division capacity were observed in some patients with CVID [40]. Our flow cytometry and RNA seq analyses on cTfh cells identified a group of CVID patients that was characterized by pronounced splenomegaly and lymphadenopathy and a more severe clinical phenotype. Our data suggest that Tfh phenotyping can be used to identify patients with a higher risk for immunoaging, dysregulation, shortened telomeres, and perhaps those carrying defects in DNA synthesis and repair. We found that a cTfh cell signature (high levels of PD-1 and Th1 polarization) correlated with plasma CXCL13 levels and $CD21^{lo}CD38^{lo}$ age-related B cells, suggesting the use of Tfh1, PD-1, and CXCL13 as potential biomarkers for this form of CVID. Additional studies in larger cohorts of patients will be required to establish the set of biomarkers that define this form of CVID and direct future therapeutic lines of research.

Tfh cells are pivotal players during the GC reaction and the production of high affinity, long-lived antibody responses [41]. In our CVID patients, cTfh cells, especially those from Group A, do not retain B cell helper activity as evidenced by their reduced ability to promote plasmablast differentiation and IgG/IgM production. Possibly, increased Tfh apoptosis is an intrinsic defect in CVID Group A patients that might contribute to poor support of B cell responses in vitro and in vivo. Additionally, the Th1 phenotype of Tfh cells played a role in preventing efficient GC responses and class switching, as the addition of IFNγ was shown to reduce IgG and IgA production in T/B co-cultures [11]. There is also evidence from previous clinical settings, i.e., HIV and CVID, that Tfh1 cells are less effective B cell helpers in comparison to their $CXCR3^{-}$ Tfh counterparts [42–44]. Interestingly, a predominant Tfh1 cell immunophenotype has been detected in several autoimmune diseases and syndromes [26, 45–47], suggesting that excessive IFNγ production in GC might promote AAb production.

A possible explanation for the observed immunophenotype and premature immunoaging derived from our genetic analysis. Monoallelic variants and polymorphisms in *RTEL1* were present in four patients with $cTfh1^{hi}Tfh17^{lo}PD\text{-}1^{hi}CXCL13^{hi}$ immunophenotype. RTEL1 has been proposed to dismantle T-loops during replication thus preventing catastrophic cleavage of telomeres as a whole extra-chromosomal T-circle [48]. Previous observations indicated that heterozygous *RTEL1* mutations are associated with premature telomere shortening despite the presence of a functional wild-type allele in vivo [32, 49]. Furthermore, Speckmann et al. showed that the immunological and clinical phenotype is very much mutation/variant-dependent but, overall, premature telomere shortening is a common feature [32]. CVID patients with *RTEL1* variants exhibited very short telomeres in their lymphocytes. Their cTfh cells expressed genes involved in DNA synthesis and repair, telomere maintenance, apoptosis, and exhaustion. Furthermore, RTEL1 expression was observed in tonsillar germinal center Tfh cells. We, therefore, assumed that the observed CVID phenotype in Group A patients with *RTEL1* variants may result in Tfh-cell replicative senescence and exhaustion also in the context of repeated activation due to chronic pathogen exposure. Hence, premature aging and Tfh apoptosis could have been the consequence and/or the underlying mechanism of this form of CVID.

RTEL1 expression was also detected in GC B cells. Tonsil-isolated centrocytes and centroblasts expressed similar levels of RTEL1. Interestingly, V(D)J recombination efficiency in RTEL1 deficiency [32] was previously found unaffected and comparable to HC suggesting a normal B-lymphocyte development in the GC and, possibly regular production of PCs. Possibly, RTEL1 mediates proliferative senescence also in mature B cells due to its essential role in DNA replication, homologous recombination, and telomere maintenance [50]. Due to its well-documented role in $CD34^{+}$ hematopoietic stem cells, RTEL1 deficiency may have contributed to B cell failure and hypogammaglobulinemia via proliferative exhaustion of the hematopoietic stem cell compartment. In future studies, we hope to be able to address the bone marrow compartment in our *RTEL1* affected cohort.

Interestingly, Bcl-6, the master regulator of the GC B and Tfh cell lineage, is located on chromosome 3q27 at the telomere proximity [51]. *RTEL1* is also located at the telomere proximity of chromosome 20. Recent studies have suggested that telomere length regulates the expression of genes that are located up to 10 Mb away from the telomere long before telomeres become short enough to produce a DNA damage response (senescence) [52, 53]. This suggests that excessive telomere shortening could have played a role in immune cell fitness through another and till today unexplored mechanism leading to this form of CVID.

High frequency of $CD57^{+}$ and $PD\text{-}1^{+}$ CD4 and CD8 T cells were observed in the spleen of one RTEL1 affected patient. CD57 is a marker of GC Tfh cells [54] but also a marker of T-cell replicative senescence associated with short telomeres [55]. $CD57^{+}$ T cells are characterized by an inability to undergo new cell-division cycles despite preserved ability to secrete cytokines after antigen encounter [55, 56]. This finding is in line with the immunophenotype of circulating T cells, where the percentage of cTfh and cTconv expressing senescent and apoptotic markers was elevated.

Interestingly, Klocperk et al. identified a population of follicular CD8 T cells in the lymph nodes of patients with CVID who clinically were characterized by lymphadenopathy. These follicular CD8 T cells also displayed senescence-associated (CD57) features suggesting they were exhausted [57].

Group A patients showed high levels of cytokines involved in inflammatory response in their serum (e.g., IFN-γ, IL-2R, MDC, MIP3-α, SDF-1α). However, intracellular cytokine analysis showed that Tfh cells from Group A CVID patients produced significantly lower amounts of cytokines as compared to HC. These data, along with their transcriptomic landscape, suggest that Group A CVID Tfh cells display a more activated phenotype while, in reality, are less functional. It is possible that in these patients, chronic exposure to pathogens perpetuates a pathogenic GC response where Tfh cells become activated, engage in futile interactions with B cells but end up "aging" faster due to RTEL1 variants.

In conclusion, by characterizing the phenotype and transcriptome of circulating Tfh cells in patients with CVID, we were able to identify a group of patients with specific clinical and immunological characteristics most possibly influenced by the presence of pathogenic variants/polymorphisms in *RTEL1* and/or related pathways. Despite the limitation of a very small sample size, our data suggest that a cTfh1^{hi}Tfh17^{lo}PD-1^{hi}CXCL13^{hi} immunophenotype and short lymphocyte telomere length could be used as indicators for genetic testing of *RTEL1* and possibly other DKC causing genes (*TERT*, *DKC1*, *NHP2*, *TERC*, etc.) in patients with CVID. Further studies will be required to better understand the contribution of *RTEL1* in Tfh and B cell development, function, and interactions, and whether the alterations seen in CVID patients with *RTEL1* variants are genetically-driven and/or secondary to infections and chronic immune stimulation.

Materials and methods

Study cohort

The study encompassed 27 patients that satisfied the following inclusion criteria: increased susceptibility to infection, autoimmune manifestations, granulomatous disease, unexplained polyclonal lymphoproliferation, affected family member with antibody deficiency (low IgA or IgM or IgG or panhypogammaglobulinemia), poor antibody response to vaccines (and/or absent isohaemagglutinins), low amount of switched memory B cells, diagnosis established after the 4th year of life, no evidence of profound T-cell deficiency (based on CD4 numbers per microliter: 2–6 years<300, 6–12 years<250, >12 years<200), % naive CD4: 2–6 years<25%, 6–16 years<20%, >16 years<10%), and altered T-cell proliferation [58]. CVID was diagnosed according to ESID criteria [59]. The study cohort was enrolled in a study conducted at San Raffaele Hospital (HSR) in Milan and was constituted by patients diagnosed at HSR or referred from other centers of the Italian "Associazione Italiana Ematologia Oncologia Pediatrica-Italian Primary Immunodeficiencies Network (AIEOP-IPINet)" (Federico II University of Naples, Ancona University, Bologna University, University of Rome Tor Vergata and Pediatric Hospital Bambin Gesù, Parma Hospital, Meyer Pediatric Hospital in Florence, Alessandria Hospital, Varese Hospital, University of Brescia, and Regina Margherita Hospital in Turin). The cohort was composed of 16 adults (mean age 36 years, age range 20–63 years) and 11 children (mean age 13 years, age range 6–17 years) (Table 1). Blood and tissues samples for the study were collected between February 2016 and January 2020, they were compared with 106 age-matched control subjects, 67 of which were adults (mean age 27 years, age range 18–52 years) and 39 children (mean age 11 years, age range 2–16 years) (Table 1, Supporting Information Table S3). Spleen tissue was collected from the pancreata of nondiabetic brain-dead multiorgan donors received at the Islet Isolation Facility of San Raffaele Hospital, following the recommendation approved by the local ethics committee. Tonsils were collected from pediatric donors as previously described [60]. Collection of biological specimens was performed after subjects or parents' signature of informed consent for biological sample collection, including genetic analyses, in the context of protocols approved by the Ethical Committee of HSR (Tiget06, Tiget09, and DRI004 protocols).

Sample collection, cell staining, and flow cytometry

FACS stainings were performed on PBMC, whole blood (EDTA), and spleen. PBMC were isolated from heparinized blood by Ficoll density gradient centrifugation using Lymphoprep (Stemcell). Surface staining was performed in fresh isolated PBMC with a panel of mAbs including CD45RA-PE (HI100, Miltenyi Biotec), CD4-PerCP (VIT4, Miltenyi Biotec), CD25-APC (2A3, BD Biosciences), PD-1-PECy7 (eBioJ105, eBiosciences), CD3-APC-Vio770 (BW264/56, Miltenyi Biotec), CXCR5-Brilliant Violet 421 (J252D4, BioLegend), CD19-PO (SJ25C1, BD Biosciences), CD14-VioGreen (TUK4, Miltenyi Biotec), CD8-VioGreen (BW135/80, Miltenyi Biotec) (Supporting Information Table S4, staining panel A). Cells were fixed and permeabilized for intracellular staining with the FoxP3/Transcription Factor Staining Buffer Set (eBioscience) prior to staining with FoxP3-Alexa Fluor 488 (259D, BD Biosciences) (Supporting Information Table S4, staining panel A).

Surface staining was performed in whole blood (EDTA) with two panels of mAbs. The first panel consisted of CD45RA-FITC (T6D11, Miltenyi Biotec), CD4-PE (REA623, Miltenyi Biotec), CCR6-PerCP (G034E3, BioLegend), CXCR3-APC (1C6, BD Biosciences), ICOS-PECy7 (ISA-3, Invitrogen), CD3-APC-Vio770 (BW264/56, Miltenyi Biotec), CXCR5- Brilliant Violet 421 (J252D4, BioLegend), CD45-Brilliant Violet 510 (HI30, BioLegend) (Supporting Information Table S4, staining panel B). The second panel consisted of: CD45RA-FITC (T6D11, Miltenyi Biotec), PD1-PE (J43, ThermoFisher), CD4-PerCP (VIT4, Miltenyi Biotec), CXCR3-APC (1C6, BD Biosciences), ICOS-PECy7 (ISA-3, Invitrogen), CD3-APC-Vio770 (BW264/56, Miltenyi Biotec),

CXCR5-Brilliant Violet 421 (J252D4, BioLegend), CD45-Brilliant Violet 510 (HI30, BioLegend) (Supporting Information Table S4, staining panel C).

B cell staining was performed on frozen PBMC after thawing in complete medium (RPMI 10% FBS, PS/G 1X) containing DNase I (Calbiochem, cod 260913) for 10 min at 37°C. 2×10^5 PBMC were stained with the following mix of mAbs, as previously described [61, 62]: CD27-APC (M-T27, BD Biosciences), CD19-PECy7 (SJ 25C1, BD Biosciences), CD21-PE (B-LY4, BD Biosciences), CD38-PerCP5.5 (HIT2, BD Biosciences), CD24-Pacific Blue (SN3, EXBIO), IgD-biotinylated (IA6-2, BD Bioscience), IgM-FITC (G20-127, BD Biosciences), IgG-FITC (polyclonal, Jackson Immunoresearch), IgA-FITC (polyclonal, Jackson Immunoresearch), and Streptavidin-Pacific Orange (ThermoFisher) (Supporting Information Table S5, staining panels A–C).

Single-cell suspensions from the spleen were prepared as previously described [63]. B cell and Tfh cell staining was performed on frozen splenocytes as described above (Supporting Information Table S5, staining panels A–D). Cells were acquired on FACS CantoII (BD) and analyzed with FlowJo (Tree Star) software.

Single-cell suspensions from the tonsil were prepared as already described [64]. Sorting of CCs, CBs, and Tfh cells from tonsils ($n = 3$) was performed on frozen cells in complete medium (RPMI 10% FBS, PS/G 1X). Cells were stained with the following mix of mAbs, as previously described [26, 27]: CD3-APC-Cy7 (BW264/56, Miltenyi Biotec), CD4-PerCP (VIT4, Miltenyi Biotec), CXCR5-Brilliant Violet 421 (J252D4, BioLegend), PD-1-PE (J43, ThermoFisher), CD27-APC (M-T27, BD Biosciences), CD38-PerCPCy5.5 (HIT2, BD Biosciences), CD20-FITC (2H7, BD Biosciences), CXCR4-PECy7 (12G5, Miltenyi Biotec) (Supporting Information Table S5, staining panels E). Cells were sorted on FACS Aria Fusion (BD) and analyzed with FlowJo (Tree Star) software. We have adhered to the guidelines described for the use of flow cytometry and cell sorting [65].

Apoptosis analysis

PBMC isolated from CVID patients and HC were stained with surface antibodies against CD45RA-FITC (REA1047, Miltenyi Biotec), CD3-PE (SK7, BD bioscience), CD4-PO (VIT4, Miltenyi Biotec), CXCR5-Brilliant Violet 421 (J252D4, BioLegend), CD25-APC (BC96, BioLegend) (Supporting Information Table S4, staining panel D) and FACS-sorted into cTfh ($CD4^+CD45RA^-CXCR5^-$), T naïve ($CD4^+CD45RA^+$), and Tconv ($CD4^+CD45RA^-CXCR5^-$) (FACS Aria Fusion [BD]). cTfh, T naïve, and Tconv, once isolated, were seeded in a 96-wells plate, activated with anti-CD3/CD28 beads (1:3 ratio, cells:beads) in complete medium (RPMI 10%FBS, PS/G) and incubated for 4 days at 37°C. At the end of incubation, cells were stained with Annexin V/propidium iodine (PI) following the FITC Annexin-V Apoptosis Detection Kit I BD Pharmingen (Cat. 556547) protocol (Supporting Information Table S4, staining panel E). Cells were acquired on FACS CantoII (BD) and analyzed with FlowJo (Tree Star) software.

B cell helper assay

PBMC were sorted into $CD19^+CD38^-CD27^-$ naive B cells, $CD19^+CD38^-CD27^+$ memory B cells, and $CXCR5^+$ $CD25^-$ Tfh cells. Before sorting, PBMC were stained with a panel of mAbs that consisted of: CD19-FITC (4G7, BD Biosciences), CD27-PE (L128, BD Biosciences), CD25-APC (2A3, BD Biosciences), CD4-PE-Vio770 (M-T321, Miltenyi Biotec), CXCR5-Brilliant Violet 421 (J252D4, BioLegend), and sorted using a FACSAria Fusion sorter cytometer (Becton Dickinson) (Supporting Information Table S4, panel F). B cells (3×10^4) were co-cultured with an equal number of $CXCR5^+$ $CD25^-$ sorted Tfh cells and stimulated with Staphylococcal enterotoxin B (100 ng/mL, Sigma-Aldrich) in complete RPMI. On culture day 7, the frequency of plasmablasts $CD38^+CD20^{low}$ was analyzed by flow cytometry. Culture supernatant IgM and IgG concentrations were determined by ELISA assay (Human IgM and IgG Uncoated ELISA Kit, Invitrogen by Thermo Fisher Scientific, Cat. No. 88-50620-22 and 88-50550-22) according to the manufacturer's instructions.

Senescence analysis

Fluorescent senescence-associated-β-galactosidase (SA-β-Gal) staining with 5-dodecanoylaminofluorescein Di-β-D-galactopyranoside (C12FDG)

T cells sorted subfractions Tfh (CD4+CD45RA-CXCR5−), (non-Tfh) Tconv (CD4+CD45RA-CXCR5−), and T naïve (CD4+CD45RA+) were seeded at the concentration of 5 × 105 CD34+ cells/mL and incubated with 150 μM Chloroquin for 1h at 37°C to induce lysosomal alkalinization. Then, cells were stained with 16.66 μM of C12FDG (ThermoFisher, Cat. N. D2893) for 30 min at 37°C. After washing with PBS, fluorescence was acquired at FACSCanto II and the collected data were analyzed using the FlowJo (Tree Star) software.

CDKN2A (p16) intracellular staining

A total of 50,000 T-cells sorted subfractions Tfh (CD45RA-CXCR5+ CD25−), (non-Tfh) Tconv (CD45RA-CXCR5− CD25−) and T naïve (CD4+CD45RA−) were washed in FACS Buffer (PBS+2%FBS) at 1600 rpm for 5 min. Then, cells were fixed with 100 μL of 4% PFA for 15 min at room temperature, washed with FACS buffer, and resuspended in 100 μL of 1× Saponin-based permeabilization for 30 min. Cells were then incubated overnight with p16 primary antibody (Purified anti-CDKN2A (p16) [15C10C30], Biolegend cat. N. 675602) diluted 1:500 in X Saponin-based permeabilization. After washing with FACS buffer, cells were stained with Goat anti-Mouse IgG2a Secondary Antibody, Alexa Fluor 647 (ThermoFisher, Cat. N. A-21241) for 45–60 min. Data were acquired at FACSCanto II and analyzed using the FlowJo (Tree Star) software.

CXCL13 ELISA assay

CXCL13 was evaluated in plasma EDTA by ELISA (Human CXCL13/BLC/BCA-1 Quantikine ELISA Kit, R & D Systems) following the manufacturer's instructions. To collect plasma, whole PB (EDTA) was centrifuged at 1000 rpm for 15 min. Plasma was further centrifuged at 13000 rpm for 10 min to remove debris.

RNA and DNA extraction

Sorted circulating Tfh cells were resuspended in 200 uL of Trizol (Ambion) and frozen at −80°C. After thawing, 100 uL of chloroform was added and RNA was extracted using the RNeasy Mini Kit (QIAGEN) with a small modification as exemplified here: after incubation for 2 min at RT, samples were centrifuged at 12000*g* for 15 min at 4°C. The transparent upper phase was transferred to a new tube and an equal volume of 70% ethanol was added. The samples were transferred to a RNeasy Mini spin column and centrifuged for 15 s at 8000 *g*. 350 μL Buffer RW1 was added to the column and spinned down 15 s at 8000*g*. DNases were inactivated using a mix consisting of 10 μL QIAGEN DNase I with 70 uL Buffer RDD. After an incubation of 30 min at RT with the DNase mix, a second wash was carried out with Buffer RW1. Subsequently, RNA was washed twice with Buffer RPE. Finally, RNA was eluted with 30 μL RNase-free water. DNA was extracted from 200 μL whole blood (EDTA) using the QIAmp DNA blood mini kit according to the manufacturer's instructions (Qiagen). RNA and DNA concentrations were quantified by NanoDrop 8000 (Thermo Scientific).

RNA sequencing and analysis

RNA-seq data were trimmed to remove Illumina adapters and low-quality reads using cutadapt.

Sequences were then aligned to the human reference genome (GRCh38/hg38) using STAR, with standard input parameters. Gene counts were produced using Subread featureCounts, using Genecode v31 as reference. Transcript counts were processed using edgeR, using standard protocols as reported in the manual. Differential expression was determined considering *p* values corrected by FDR including sex as a covariate. Heatmaps were produced with pheatmap R package, whereas volcano and scatter plots were produced with the ggplot2 R package.

Immunohistochemistry

Formalin-fixed, paraffin-embedded tissue 3–4 μm thick sections from spleen specimens were stained with hematoxylin–eosin and underwent histopathological assessment from certified pathologists of our hospital. For immunohistochemistry, the following antibodies were applied: CD20, CD3, and Bcl-2 (Supporting Information Table S6 for clones and dilutions). Immunohistochemistry was performed using the standard avidin-biotin-peroxidase complex method, as described elsewhere [66]. The immunostaining for Bcl-6 (clone GI 191E/A8) was performed with an automated immunostainer (Benchmark XT, Ventana Medical Systems) after heat-induced epitope retrieval, which was carried out using Ventana cell conditioning buffer 1 (CC1) for 60 min.

Images were obtained on a Nikkon microscope system with 40 × (NA 1.3) and 20 × (NA 0.75) objectives.

Genomic studies

Whole exome sequencing

The WES of genomic DNA was performed by *Genomnia* (http://www.genomnia.com/). DNA libraries were sequenced on a Hiseq 4000 (Illumina) for paired-end 150 bp reads. Sequencing reads were mapped to the reference human genome (UCSC hg19 and hg38) with the Torrent Suite (5.10.0). The bam files generated from two chips were merged with the Combine Alignments utility of the Torrent Suite. The samples were analyzed with the workflow Ion Report Ampliseq exome single sample (germline) version 5.6. The quality of the sequencing was verified with the fastqc software v.0.10.1 e samstat v.1.08.

Candidate variants responsible for the disease

The variants noted by Ion Reporter were analyzed highlighting those that fulfilled the following criteria:

- Quality >40 (to exclude false positives)
- Minor allele frequency MAF < 1% ("rare variants") or < 5% ("uncommon variants")
- Variants of candidate genes
- Non-synonymous exonic variants, with a strong impact on the protein sequence, i.e.: indels causing frameshift; variants introducing or eliminating stop codons; missense variants predicted by SIFT and/or PolyPhen as potentially deleterious for the structure and functionality of the protein; variations on splicing sites.

Candidate variants were screened based on the phenotypes and any known inheritance pattern of the patients. When the cases were sporadic without a familial inheritance tendency, we first hypothesized that the patients had a monogenic disorder with an autosomal recessive pattern caused by a homozygous or compound heterozygous inheritance or with a de novo or heterozygous dominant mutation with incomplete penetrance. If no causative mutations were found, we considered the case as a complex form of CVID. Afterward, top likely disease-associated variants were validated by Sanger sequencing. Supporting Information Table S1 includes the gene pipeline used for the discovery of possible causative mutations of CVID designed based on known genes or candidates published in the literature, IUIS classification, as previously shown [30].

Oligonucleotides for PCR and Sanger sequencing

Primers used for amplification and sequencing of genomic DNA are shown in Supporting Information Table S7. Amplified DNA fragments were purified using QIAquick PCR Purification Kit (QIAGEN), according to the manufacturer's instructions. At the end of the purification 400 ng of DNA were sent to sequence with the Sanger method to Eurofins Scientific.

Sanger sequencing analysis

The electropherogram of each sample obtained from the Sanger sequencing was analyzed using the FinchTV program and Nucleotide BLAST, a search nucleotide databases collection.

Telomere length

Telomere testing was performed by Repeat Diagnostics Inc.

RTEL1 gene expression assay

RNA was extracted from 2×10^5 sorted CC, CB, and Tfh cells (RNeasy Micro Kit, Qiagen), quantified (NanoDrop 2000, ThermoFisher), and retrotranscribed (High-Capacity cDNA Reverse Transcription Kit, ThermoFisher). Cells were sorted as follow; Tfh cells as $CD3^+CD20^-$, $CD4^+$, $PD\text{-}1^+CXCR5^+$; CCs as $CD20^+CD3^-$, $CD27^-CD38^{dim}$, $CXCR4^-$; CBs as $CD20^+CD3^-$, $CD27^-CD38^{dim}$, $CXCR4^+$. The complete antibody mix is described in Supporting Information Table S5, panel E. Then, gene expression was performed in duplicates using a Droplet Digital PCR system (Bio-Rad) following the manufacturer's instructions (BioRad Droplet Digital PCR Applications Guide, Bulletin_6407). The following ddPCR gene expression assay was used in duplex: AL353715.1 – RTEL1, Human, FAM (dHsaCPE5191681); XBP1, Human, HEX (dHsaCPE5033517); Bcl-6, Human, HEX (dHsaCPE5034897); HPRT1, Human, FAM (dHsaCPE5192871). Data were analyzed with QuantaSoft 1.7.4.0917 (Bio-Rad) software.

Statistics

Statistical analyses were performed using GraphPad Prism software version 7. Quantitative data are expressed as median (range), and categorical data are expressed as percentage (percentage). Comparisons between two groups were performed using nonparametric Mann–Whitney *U* tests. Comparisons among > 2 groups were performed using the ANOVA test. Relationships between different parameters were examined using the Pearson correlation coefficient. Statistical significance of clinical data was assessed with the Fisher exact test. p values ≤ 0.05 were considered significant and indicated with an asterisk. **, ***, and **** stand for p values ≤ 0.01, ≤ 0.001 and ≤ 0.0001, respectively.

Acknowledgments: This work was supported from 5 × 1000 OSR PILOT & SEED GRANT to GF & MPC. We would like to thank our past lab members for their contribution. Moreover, we acknowledge the nurses, the patients, and their families.
Open access funding provided by BIBLIOSAN.

Conflict of interest: The authors declare no commercial or financial conflict of interest.

Data availability statement: The data that support the findings of this study are available from the corresponding author upon reasonable request.

Peer review: The peer review history for this article is available at https://publons.com/publon/10.1002/eji.202149480.

References

1 **Chapel, H., Lucas, M., Lee, M., Bjorkander, J., Webster, D., Grimbacher, B., Fieschi, C. et al.**, Common variable immunodeficiency disorders: division into distinct clinical phenotypes. *Blood*. 2008. **112**: 277–286.

2 **Tam, J. S. and Routes, J. M.** Common variable immunodeficiency. *Am. J. Rhinol. Allergy*. 2013. **27**: 260–265.

3 **Fieschi, C., Malphettes, M. and Galicier, L.** Adult-onset primary hypogammaglobulinemia. *Presse. Med*. 2006. **35**: 887–894.

4 **Gathmann, B., Mahlaoui, N., Gérard, L., Oksenhendler, E., Warnatz, K., Schulze, I., Kindle, G. et al.**, Clinical picture and treatment of 2212 patients with common variable immunodeficiency. *J. Allergy. Clin. Immunol*. 2014. **134**: 117–137.

5 **Wood, P., Stanworth, S., Burton, J., Jones, A., Peckham, D. G., Green, T., Hyde, C. et al.**, Recognition, clinical diagnosis and management of patients with primary antibody deficiencies: A systematic review. *Clin. Exp. Immunol*. 2007. **149**: 410–423.

6 **Van De Ven, A. A. J. M. and Warnatz, K.** The autoimmune conundrum in common variable immunodeficiency disorders. *Curr. Opin. Allergy Clin. Immunol*. 2015. **15**: 514–524.

7 **Gomes Ochtrop, M. L., Goldacker, S., May, A. M., Rizzi, M., Draeger, R., Hauschke, D., Stehfest, C. et al.**, T and B lymphocyte abnormalities in bone marrow biopsies of common variable immunodeficiency. *Blood*. 2011. **118**: 309–318.

8 **Warnatz, K. and Voll, R. E.** Pathogenesis of autoimmunity in common variable immunodeficiency. *Front. Immunol.* 2012. **3**: 1–6.

9 **Taubenheim, N., von Hornung, M., Durandy, A., Warnatz, K., Corcoran, L., Peter, H. -. H. and Eibel, H.** Defined Blocks in Terminal Plasma Cell Differentiation of Common Variable Immunodeficiency Patients. *J. Immunol*. 2005. **175**: 5498–5503.

10 **Deenick, E. K. and Ma, C. S.** The regulation and role of T follicular helper cells in immunity. *Immunology*. 2011. **134**: 361–367.

11 **Le Saos-Patrinos, C., Loizon, S., Blanco, P., Viallard, J. F. and Duluc, D.** Functions of Tfh Cells in Common Variable Immunodeficiency. *Front. Immunol*. 2020. **11**: 1–7.

12 **Tangye, S. G., Al-Herz, W., Bousfiha, A., Cunningham-Rundles, C., Franco, J. L., Holland, S. M., Klein, C. et al.**, The Ever-Increasing Array of Novel

Inborn Errors of Immunity: an Interim Update by the IUIS Committee. *J. Clin. Immunol*. 2021. **41**: 666–679.

13 **Amir, W. and Beard, B. T**. Role of B cells in common variable immune deficiency Sam. *Bone* 2008. **23**: 1–7. Available from: https://www.ncbi.nlm.nih.gov/pmc/articles/PMC3624763/pdf/nihms412728.pdf

14 **Yong, P. F. K., Salzer, U. and Grimbacher, B.** The role of costimulation in antibody deficiencies: ICOS and common variable immunodeficiency. *Immunol. Rev*. 2009. **229**: 101–113.

15 **Warnatz, K., Bossaller, L., Salzer, U., Skrabl-Baumgartner, A., Schwinger, W., Van Der Burg, M., van Dongen, J. J. M. et al.**, Human ICOS deficiency abrogates the germinal center reaction and provides a monogenic model for common variable immunodeficiency. *Blood* 2006. **107**: 3045–3052.

16 **Bossaller, L., Burger, J., Draeger, R., Grimbacher, B., Knoth, R., Plebani, A., Durandy, A. et al.**, ICOS Deficiency Is Associated with a Severe Reduction of CXCR5 + CD4 Germinal Center Th Cells. *J. Immunol*. 2006. **177**: 4927–4932.

17 **Kotlarz, D., Ziętara, N., Uzel, G., Weidemann, T., Braun, C. J., Diestelhorst, J., Robinson, P. N. et al.**, Loss-of-function mutations in the IL-21 receptor gene cause a primary immunodeficiency syndrome. *J. Exp. Med*. 2013. **210**: 433–443.

18 **Salzer, E., Kansu, A., Sic, H., Májek, P., Ikincioğullari, A., Dogu, F. E., Prengemann, N. K. et al.**, Early-onset inflammatory bowel disease and common variable immunodeficiency-like disease caused by IL-21 deficiency. *J. Allergy Clin. Immunol*. 2014. **133**: 1651–1671.

19 **Eastwood, D., Gilmour, K. C., Nistala, K., Meaney, C., Chapel, H., Sherrell, Z., Webster, A. D. et al.**, Prevalence of SAP gene defects in male patients diagnosed with common variable immunodeficiency. *Clin. Exp. Immunol*. 2004. **137**: 584–588.

20 **van Schouwenburg, P. A., Davenport, E. E., Kienzler, A. K., Marwah, I., Wright, B., Lucas, M., Malinauskas, T. et al.**, Application of whole genome and RNA sequencing to investigate the genomic landscape of common variable immunodeficiency disorders. *Clin. Immunol.* 2015. **160**: 301–314. Available from: http://doi.org/10.1016/j.clim.2015.05.020

21 **Simpson, N., Gatenby, P. A., Wilson, A., Malik, S., Fulcher, D. A., Tangye, S. G., Manku, H. et al.**, Expansion of circulating T cells resembling follicular helper T cells is a fixed phenotype that identifies a subset of severe systemic lupus erythematosus. *Arthritis Rheum*. 2010. **62**: 234–244.

22 **Ma, J., Zhu, C., Ma, B., Tian, J., Baidoo, S. E., Mao, C., Wu, W. et al.**, Increased frequency of circulating follicular helper T cells in patients with rheumatoid arthritis. *Clin. Dev. Immunol*. 2012. **2012**: 1–7.

23 **Bentebibel, S. E., Lopez, S., Obermoser, G., Schmitt, N., Mueller, C., Harrod, C., Flano, E. et al.**, Induction of ICOS+CXCR3+CXCR5+ T H cells correlates with antibody responses to influenza vaccination. *Sci. Transl. Med*. 2013. **5**: 1–19.

24 **Xu, M., Jiang, Y., Wang, J., Liu, D., Wang, S., Yi, H., Yang, S. et al.**, Distribution of distinct subsets of circulating T follicular helper cells in Kawasaki disease. *BMC Pediatr*. 2019. **19**: 1–9.

25 **Cunill, V., Clemente, A., Lanio, N., Barceló, C., Andreu, V., Pons, J., Ferrer, J. M. et al.**, Follicular T cells from smB- common variable immunodeficiency patients are skewed toward a Th1 phenotype. *Front. Immunol*. 2017. **8**: 1–13.

26 **Gensous, N., Charrier, M., Duluc, D., Contin-Bordes, C., Truchetet, M. E., Lazaro, E., Duffau, P. et al.**, T follicular helper cells in autoimmune disorders. *Front. Immunol*. 2018. **9**: 1–18.

27 **Cárdeno, A., Magnusson, M. K., Quiding-Järbrink, M. and Lundgren, A.** Activated T follicular helper-like cells are released into blood after oral vaccination and correlate with vaccine specific mucosal B-cell memory. *Sci. Rep*. 2018. **8**: 1–15.

28 **Cahu, J. and Sola, B.** A sensitive method to quantify senescent cancer cells. *J. Vis. Exp*. 2013. **78**: 1–6.

29 **Buj, R., Leon, K. E., Anguelov, M. A. and Aird, K. M.** Suppression of p16 alleviates the senescence-associated secretory phenotype. *Aging (Albany NY)*. 2021. **13**: 3290–3312.

30 **Cifaldi, C., Brigida, I., Barzaghi, F., Zoccolillo, M., Ferradini, V., Petricone, D., Cicalese, M. P. et al.**, Targeted NGS platforms for genetic screening and gene discovery in primary immunodeficiencies. *Front. Immunol*. 2019. **10**: 1–19.

31 **Kannengiesser, C., Borie, R., Ménard, C., Réocreux, M., Nitschké, P., Gazal, S., Mal, H. et al.**, Heterozygous RTEL1 mutations are associated with familial pulmonary fibrosis. *Eur. Respir. J.* 2015. **46**: 474–485. Available from: http://doi.org/10.1183/09031936.00040115

32 **Speckmann, C., Sahoo, S. S., Rizzi, M., Hirabayashi, S., Karow, A., Serwas, N. K., Hoemberg, M. et al.**, Clinical and molecular heterogeneity of RTEL1 deficiency. *Front Immunol*. 2017. **8**: 1–19.

33 **Deng, Z., Glousker, G., Molczan, A., Fox, A. J., Lamm, N., Dheekollu, J., Weizman, O. -. E. et al.**, Inherited mutations in the helicase RTEL1 cause telomere dysfunction and Hoyeraal-Hreidarsson syndrome. *Proc. Natl. Acad. Sci. USA* 2013. **110**: 3408–3416.

34 **LeGuen, T., Jullien, L., Touzot, F., Schertzer, M., Gaillard, L., Perderiset, M., Carpentier, W. et al.**, Human RTEL1 deficiency causes hoyeraal-hreidarsson syndrome with short telomeres and genome instability. *Hum. Mol. Genet*. 2013. **22**: 3239–3249.

35 **Glousker, G., Touzot, F., Revy, P., Tzfati, Y., Savage, S. A., Ram, G. et al.**, Unraveling the Pathogenesis of Hoyeraal-Hreidarsson Syndrome, a Complex Telomere Biology Disorder. *Br. J. Haematol*. 2016. **170**: 457–471.

36 **Bertuch, A. A.** The molecular genetics of the telomere biology disorders. *RNA Biol.* 2016. **13**: 696–706. Available from: http://doi.org/10.1080/15476286.2015.1094596

37 **Tummala, H., Walne, A., Collopy, L., Cardoso, S., De La Fuente, J., Lawson, S., Powell, J. et al.**, Poly(A)-specific ribonuclease deficiency impacts telomere biology and causes dyskeratosis congenita. *J. Clin. Invest*. 2015. **125**: 2151–2160.

38 **Savage, S. A., Giri, N., Baerlocher, G. M., Orr, N. and Lansdorp, P. M.**, Alter BP. TINF2, a component of the Shelterin telomere protection complex, is mutated in dyskeratosis congenita. *Am. J. Hum. Genet*. 2008. **82**: 501–509.

39 **Quispe-Tintaya, W.** Common variable immune deficiency: dissection of the variable. *Physiol. Behav*. 2017. **176**: 139–148.

40 **Visentini, M., Cagliuso, M., Conti, V., Carbonari, M., Mancaniello, D., Cibati, M., Siciliano, G. et al.**, Telomere-dependent replicative senescence of B and T cells from patients with type 1a common variable immunodeficiency. *Eur. J. Immunol*. 2011. **41**: 854–862.

41 **Stebegg, M., Kumar, S. D., Silva-Cayetano, A., Fonseca, V. R., Linterman, M. A. and Graca, L.** Regulation of the germinal center response. *Front. Immunol.* 2018. **9**: 1–13.

42 **Kudryavtsev, I., Serebriakova, M., Starshinova, A., Zinchenko, Y., Basantsova, N., Malkova, A., Soprun, L. et al.**, Imbalance in B cell and T follicular helper cell subsets in pulmonary sarcoidosis. *Sci. Rep*. 2020. **10**: 1–10.

43 **Zhang, J., Liu, W., Wen, B., Xie, T., Tang, P., Hu, Y., Huang, L. et al.**, Circulating CXCR3+ Tfh cells positively correlate with neutralizing antibody responses in HCV-infected patients. *Sci. Rep*. 2019. **9**: 1–10.

44 **Crotty, S.** T follicular helper cell differentiation, function, and roles in disease. *Immunity*. 2014. **41**: 529–542. Available from: http://doi.org/10.1016/j.immuni.2014.10.004

45 **Ottaviano, G., Gerosa, J., Santini, M., De Leo, P., Vecchione, A., Jofra, T., Trimarchi, C. et al.**, A prevalent CXCR3+ phenotype of circulating follicular helper T cells indicates humoral dysregulation in children with down syndrome. *J. Clin. Immunol*. 2020. **40**: 447–455.

46 **Unger, S., Seidl, M., van Schouwenburg, P., Rakhmanov, M., Bulashevska, A., Frede, N., Grimbacher, B. et al.**, The TH1 phenotype of

follicular helper T cells indicates an IFN-γ–associated immune dysregulation in patients with CD21low common variable immunodeficiency. *J. Allergy. Clin. Immunol*. 2018. **141**: 730–740. Available from: http://doi.org/10.1016/j.jaci.2017.04.041

47 **Turpin, D., Furudoi, A., Parrens, M., Blanco, P., Viallard, J. F. and Duluc, D.** Increase of follicular helper T cells skewed toward a Th1 profile in CVID patients with non-infectious clinical complications. *Clin. Immunol*. 2018. **197**: 130–138.

48 **Vannier, J. B., Pavicic-Kaltenbrunner, V., Petalcorin, M. I. R., Ding, H. and Boulton, S. J.** RTEL1 dismantles T loops and counteracts telomeric G4-DNA to maintain telomere integrity. *Cell* 2012. **149**: 795–806. Available from: http://doi.org/10.1016/j.cell.2012.03.030

49 **Marsh, J. W., Gutierrez-Rodrigues, F., Cooper, J., Jiang, J., Gandhi, S., Kajigaya, S., Feng, X. et al.**, Heterozygous RTEL1 variants in bone marrow failure and myeloid neoplasms. *Blood Adv*. 2018. **2**: 36–48.

50 **Hwang, J. K., Alt, F. W. and Yeap, L. -. S.** Related mechanisms of antibody somatic hypermutation and class switch recombination. *Microbiol. Spectr*. 2015. **3**: 1–35.

51 **Walker, S. R., Nelson, E. A. and Frank, D. A.** STAT5 represses BCL6 expression by binding to a regulatory region frequently mutated in lymphomas. *Oncogene*. 2007. **26**: 224–233.

52 **Flanary, B.** Regulation of murine telomere length via Rtel. *Rejuvenat. Res*. 2004. **7**: 168–170.

53 **Robin, J. D., Ludlow, A. T., Batten, K., Magdinier, F., Stadler, G., Wagner, K. R., Shay, J. W. et al.**, Telomere position effect: regulation of gene expression with progressive telomere shortening over long distances. *Genes Dev*. 2014. **28**: 2464–2476.

54 **Wallin, E. F., Jolly, E. C., Suchánek, O., Bradley, J. A., Espéli, M., Jayne, D. R. W., Linterman, M. A. et al.**, Human T-follicular helper and T-follicular regulatory cell maintenance is independent of germinal centers. *Blood* 2014. **124**: 2666–2674.

55 **Brenchley, J. M., Karandikar, N. J., Betts, M. R., Ambrozak, D. R., Hill, B. J., Crotty, L. E., Casazza, J. P. et al.**, Expression of CD57 defines replicative senescence and antigen-induced apoptotic death of CD8+ T cells. *Blood*. 2003. **101**: 2711–2720.

56 **Focosi, D., Bestagno, M., Burrone, O. and Petrini, M.** CD57 + T lymphocytes and functional immune deficiency. *J. Leukoc. Biol*. 2010. **87**: 107–116.

57 **Klocperk, A., Unger, S., Friedmann, D., Seidl, M., Zoldan, K., Pfeiffer, J., Hausmann, O. et al.**, Exhausted phenotype of follicular CD8 T cells in CVID. *J. Allergy. Clin. Immunol*. 2020. **146**: 912–915. e13.

58 M. Christopher AMLS. Differentiation of common variable immunodeficiency from Ig G deficiency Charles. *Physiol Behav*. 2016. **176**: 100–106.

59 **Seidel, M. G., Kindle, G., Gathmann, B., Quinti, I., Buckland, M., van Montfrans, J., Scheible, R. et al.**, The European Society for Immunodeficiencies (ESID) registry working definitions for the clinical diagnosis of inborn errors of immunity. *J. Allergy Clin. Immunol. Pract*. 2019. **7**: 1763–1770.

60 **Di Fonte, R., Baronio, M., Plebani, A., Lougaris, V. and Fousteri, G.** Reduced germinal center follicular helper T cells but normal follicular regulatory T cells in the tonsils of a patient with a mutation in the PI3KR1 gene. *Clin. Immunol*. 2016. **164**: 43–44. Available from: http://doi.org/10.1016/j.clim.2016.01.016

61 **Richardson, C. T., Slack, M. A., Dhillon, G., Marcus, C. Z., Barnard, J., Palanichamy, A., Sanz, I. et al.**, Failure of B cell tolerance in CVID. *Front. Immunol*. 2019. **10**: 1–9.

62 **Bukowska-Straková, K., Kowalczyk, D., Baran, J., Siedlar, M., Kobylarz, K. and Zembala, M.** The B-cell compartment in the peripheral blood of children with different types of primary humoral immunodeficiency. *Pediatr. Res*. 2009. **66**: 28–34.

63 **Ferraro, A., Socci, C., Stabilini, A., Valle, A., Monti, P., Piemonti, L., Nano, R. et al.**, Expansion of Th17 cells and functional defects in T regulatory cells are key features of the pancreatic lymph nodes in patients with type 1 diabetes. *Diabetes*. 2011. **60**: 2903–2913.

64 **Assadian, F., Sandström, K., Laurell, G., Svensson, C., Akusjärvi, G. and Punga, T.** Efficient isolation protocol for B and T lymphocytes from human palatine tonsils. *J. Vis. Exp*. 2015. **2015**: 1–7.

65 **Cossarizza, A., Chang, H. D., Radbruch, A., Abrignani, S., Addo, R., Akdis, M., Andrä, I. et al.**, Guidelines for the use of flow cytometry and cell sorting in immunological studies (third edition). *Eur. J. Immunol*. 2021. **51**: 2708–3145.

66 **Tibiletti, M. G., Martin, V., Bernasconi, B., Del Curto, B., Pecciarini, L., Uccella, S., Pruneri, G. et al.**, BCL2, BCL6, MYC, MALT 1, and BCL10 rearrangements in nodal diffuse large B-cell lymphomas: a multicenter evaluation of a new set of fluorescent in situ hybridization probes and correlation with clinical outcome. *Hum. Pathol*. 2009. **40**: 645–652. Available from: http://doi.org/10.1016/j.humpath.2008.06.032

Abbreviations: **AICD**: activation-induced cell death · **Bcl-6**: B cell lymphoma 6 · $\mathbf{B_M}$: B memory · $\mathbf{B_N}$: B naïve · **CBs**: centroblasts · **CCs**: centrocytes · **CVID**: common variable immunodeficiency · **CXCL13**: chemokine (C-X-C motif) ligand 13 · **CXCR5**: chemokine (C-X-C motif) receptor type 5 · **DKC**: dyskeratosis congenita · **ESID**: European Society for Immunodeficiencies · **GCs**: germinal centers · **GSEA**: gene set enrichment analysis · **HC**: healthy control · **ICOS**: inducible T cell co-stimulator · **PAD**: primary antibody deficiency · **PD-1**: programmed cell death protein 1 · **RTEL1**: regulator of telomere elongation helicase 1 · **SCID**: Severe combined immunodeficiency · **Tfh**: T follicular helper · **Tfr**: T follicular regulatory · **Treg**: T regulatory · **WES**: whole-exome sequencing

Full correspondence: Georgia Fousteri, Ph.D., Division of Immunology, Transplantation, and Infectious Diseases, Diabetes Research Institute, IRCCS San Raffaele Hospital, Milan, Italy.
e-mail: fousteri.georgia@hsr.it

Received: 29/6/2021
Revised: 8/2/2022
Accepted: 9/5/2022
Accepted article online: 13/5/2022